

# Representation of phosphorus cycle in Joint UK Land Environment Simulator (vn5.5\_JULES-CNP)

Mahdi (André) Nakhavali<sup>1</sup>, Lina M. Mercado<sup>1,2</sup>, Iain P. Hartley<sup>1</sup>, Stephen Sitch<sup>1</sup>, Fernanda V Cunha<sup>3</sup>, Raffaello di Ponzio<sup>3</sup>, Laynara F. Lugli<sup>3</sup>, Carlos A. Quesada<sup>3</sup>, Kelly M. Andersen<sup>1,4,5</sup>, Sarah E. Chadburn<sup>6</sup>, Andy J. Wiltshire<sup>1,7</sup>, Douglas B. Clark<sup>2</sup>, Gyovanni Ribeiro<sup>3</sup>, Lara Siebert<sup>3</sup>, Anna C. M. Moraes<sup>3</sup>, Jéssica Schmeisk Rosa<sup>3</sup>, Rafael Assis<sup>3</sup> and José L. Camargo<sup>3</sup>

<sup>1</sup>University of Exeter, College of Life and Environmental Sciences, Exeter, EX4 4QE, United Kingdom

<sup>2</sup>UK Centre for Ecology and Hydrology, Wallingford, OX10 8BB, United Kingdom

<sup>3</sup>Coordination of Environmental Dynamics, National Institute of Amazonian Research, Manaus, AM 69060-062, Brazil

<sup>4</sup>University of Edinburgh, School of Geosciences, Edinburgh, EH8 9AB, UK

<sup>5</sup>Nanyang Technological University, Asian School of the Environment, Singapore, 639798, Singapore

<sup>6</sup>College of Engineering, Mathematics, and Physical Sciences, University of Exeter, Exeter, EX4 4QE, United Kingdom

<sup>7</sup>Met Office Hadley Centre, Exeter, Devon, EX1 3PB, United Kingdom

Correspondence to: Mahdi (André) Nakhavali ([m.nakhavali@exeter.ac.uk](mailto:m.nakhavali@exeter.ac.uk))

## Abstract

Most Land Surface Models (LSMs), the land components of Earth system models (ESMs), include representation of nitrogen (N) limitation on ecosystem productivity. However only few of these models have incorporated phosphorus (P) cycling. In tropical ecosystems, this is likely to be important as N tends to be abundant but the availability of rock-derived elements, such as P, can be very low. Thus, without a representation of P cycling, tropical forest response in areas such as Amazonia to rising atmospheric CO<sub>2</sub> conditions remains highly uncertain. In this study, we introduced P dynamics and its interactions with the N and carbon (C) cycles into the Joint UK Land Environment Simulator (JULES). The new model (JULES-CNP) includes the representation of P stocks in vegetation and soil pools, as well as key processes controlling fluxes between these pools. We evaluate JULES-CNP using in situ data collected at a low fertility site in the Central Amazon, with a soil P content representative of 60% of soils across the Amazon basin, to parameterise, calibrate and evaluate JULES-CNP. Novel soil and plant P pool observations are used for parameterisation and calibration and the model is evaluated against C fluxes and stocks, and for those soil P pools not used for parameterisation/calibration. We then apply the model under elevated CO<sub>2</sub> (600 ppm) at our study site to quantify the impact of P limitation on CO<sub>2</sub> fertilization. We compare our results against the current state-of-the-art CNP models using the same methodology that was used in the AmazonFACE model intercomparison study. The model is able to reproduce the observed plant and soil P pools and fluxes used for evaluation under ambient CO<sub>2</sub>. We estimate P to limit net primary productivity (NPP) by 24% under current CO<sub>2</sub> and by 46% under elevated CO<sub>2</sub>. Under elevated CO<sub>2</sub>, biomass in simulations accounting for CNP increase by 10% relative to at contemporary CO<sub>2</sub>, although it is 5% lower compared with CN and C-only simulations. Our results highlight the potential for high P limitation and therefore lower CO<sub>2</sub> fertilization capacity in the Amazon forest with low fertility soils.

## 1. Introduction

Land ecosystems currently take up about 30% of anthropogenic CO<sub>2</sub> emissions (Friedlingstein *et al.*, 2020), thus buffering the anthropogenic increase in atmospheric CO<sub>2</sub>. Tropical forests play a major role in the land C cycle, account for about half of global net primary production (NPP)(Schimel *et al.*, 2015), and store the highest above ground carbon among all biomes (Pan *et al.*, 2011; Mitchard, 2018).

The C sink capacity of tropical forests may be constrained by nutrient availability for plant photosynthesis and growth (Vitousek and Howarth, 1991; Elser *et al.*, 2007; LeBauer and Treseder, 2008) via either P (Nordin, Högberg and Näsholm, 2001; Shen *et al.*, 2011) and N related processes (DeLuca, Keeney and McCarty, 1992; Perakis and Hedin, 2002). Global process-based models of vegetation dynamics and function suggest a continued land C sink in the tropical forests, largely attributed to the CO<sub>2</sub> fertilization effect (Sitch *et al.*, 2008; Schimel, Stephens and Fisher, 2015; Koch, Hubau and Lewis, 2021). However, many of these models typically do not consider P constraints on plant growth (Fleischer *et al.*, 2019), which is likely to be an important limiting nutrient in tropical ecosystems, characterised by old and heavily weathered soils. The importance of nutrient cycling representation in Earth System Models (ESMs), and the lack thereof, was highlighted by Hungate *et al.* (2003) and Zaehle and Dalmonech (2011), showing the significance of nitrogen inclusion in ESMs for generating more realistic estimations of the future evolution of the terrestrial C sink. However, in the Coupled Climate C Cycle Model Inter-comparison Project (C4MIP), none of the participating ESMs included N dynamics (Friedlingstein *et al.*, 2006). Seven years later, for the update in CMIP5 (Anav *et al.*, 2013), three models out of eighteen with N dynamics were included (Bentsen *et al.*, 2013; Long *et al.*, 2013; Ji *et al.*, 2014). Although much progress has been made in the inclusion of an N cycle in ESMs so far, none of the CMIP5 models included P cycling and in the most recent CMIP6, only one model includes P (ACCESSESM1.5 model) (Arora *et al.*, 2020).

The long history of soil development in tropical regions which involves the loss of rock-derived nutrients through weathering and leaching on geologic timescales (Vitousek *et al.*, 1997, 2010) results in highly weathered soils. Soil P is hypothesized to be among the key limiting nutrients to plant growth in tropical forests (Vitousek *et al.*, 1997, 2010; Hou *et al.*, 2020), unlike temperate forest where N is hypothesised to be the main constraint (Aerts and Chapin, 1999; Luo *et al.*, 2004). Low P availability in tropical soils is related to the limited un-weathered parent material or organic compounds as source of P (Walker and Syers, 1976), active sorption (Sanchez, 1977) and high occlusion (Yang and Post, 2011) which further reduce plant available P. Although N limitation can impact the terrestrial C sink response to increasing atmospheric CO<sub>2</sub> by changing plant C fixation capacity (Luo *et al.*, 2004), this can be partially ameliorated over time by input of N into the biosphere via the continuous inputs of N into ecosystems from atmospheric deposition and biological N fixation (Vitousek *et al.*, 2010). P-limitation is pervasive in natural ecosystems (Hou *et al.*, 2020) and the lack of large P inputs into ecosystems, especially those growing on highly weathered soil, may make P limitation a stronger constraint on ecosystem response to elevated CO<sub>2</sub> (eCO<sub>2</sub>) than N (Gentile *et al.*, 2012; Sardans, Rivas-Ubach and Peñuelas, 2012). This causes considerable uncertainty in predicting the future of the Amazon forest C sink (Yang *et al.*, 2014).

There is evidence to suggest P limitation on plant productivity in the Amazon forest (Malhi, 2012) where it has been shown that the younger, more fertile west and south-west Amazon soils have higher tree turnover (Phillips *et al.*, 2004; Stephenson and Van Mantgem, 2005) and stem growth rates (Malhi *et al.*, 2004) and lower above ground biomass (Baker *et al.*, 2004; Malhi *et al.*, 2006) compared to their central and eastern counterparts. Total soil P has been found as the best predictor of stem growth (Quesada *et al.*, 2010) and of total NPP (Aragão *et al.*, 2009) across this fertility gradient, and foliar P is positively related to plant photosynthetic capacity ( $V_{cmax}$  and  $J_{cmax}$ ) in these forests (Mercado *et al.*, 2011).

However, modelling studies are unable to reproduce observed spatial patterns of NPP and biomass in the Amazon due to missing information on nutrient availability and soil fertility impact on productivity (Wang, Law and Pak, 2010; Vicca *et al.*, 2012; Yang *et al.*, 2014) and due to the lack of inclusion of soil P constraints on plant productivity and function. Nevertheless, some modelling works have focused on improving process and parameter representation using the observational data of spatial variation in woody biomass residence time (Johnson *et al.*, 2016), soil texture and soil P to parameterise the maximum RuBiCo carboxylation capacity ( $V_{cmax}$ ) (Castanho *et al.*, 2013). Results from these studies successfully represent observed patterns of Amazon forest biomass growth increases with increasing soil fertility. However, the full representation of these interactions and the impact of the soil nutrient availability on biomass productivity is still missing in most of ESMs.

104 So far, several dynamic global vegetation models have been developed to represent P cycling within the soil  
105 (Yang *et al.*, 2013; Haverd *et al.*, 2018) and between plant and soils for tropical forests particularly (Yang *et al.*,  
106 2014; Zhu *et al.*, 2016; Goll *et al.*, 2017). Furthermore, a comprehensive study included several models with C-  
107 N-P cycling and their feedbacks on the atmospheric C fixation and biomass growth in Amazon forests under  
108 ambient and eCO<sub>2</sub> conditions (Fleischer *et al.*, 2019). Despite these developments, data to underpin them and  
109 their projections, particularly for the tropics, is sparse and remains challenging particularly for the Amazon  
110 forest (Reed *et al.*, 2015; Jiang *et al.*, 2019). Moreover, due to the lack of detailed measurements, the P-related  
111 processes such as ad/desorption and uptake represented in these models are under-constrained and likely  
112 oversimplified, thus the future predictions of Amazon forest responses to eCO<sub>2</sub> and climate change are  
113 uncertain. To fill this gap, in this study, we will use data collected as part of the Amazon Fertilization  
114 Experiment (AFEX), the first project that focuses on experimental soil nutrient manipulation in the Amazon,  
115 with a comprehensive data collection program covering plant ecophysiology, C stocks and fluxes, soil processes  
116 including P stocks. Thus, our model parameterization compared to prior P modelling studies includes detailed P  
117 processes representation using the site measurements.

118  
119 Here, we describe the development and implementation of the terrestrial P cycle in the Joint UK Land  
120 Environment Simulator (JULES) (Clark *et al.*, 2011), the land component of the UK Earth System Model  
121 (UKESM), following the structure of the prior N cycle development (Wiltshire *et al.*, 2021). The model  
122 (JULES-CNP) is parameterized and calibrated using novel in situ P soil and plant data from a well-studied forest  
123 site in Central Amazon near to Manaus, Brazil with soil P content representative of 60% of soils across the  
124 Amazon basin. We then evaluate the model against carbon stocks and fluxes from data sets from our study site  
125 and the nearby K34 field site. To test the model, we followed the protocol of Fleischer *et al.*, (2019), to predict  
126 nutrient limitations on land biogeochemistry under ambient and eCO<sub>2</sub>. Predictions of the CO<sub>2</sub> fertilization effect  
127 in JULES-CNP are compared to those in current versions of the model with coupled C and N cycles (JULES-  
128 CN) and with C cycle only (JULES-C).

129  
130

## 131 2. Material and methods

132  
133

### 133 2.1 JULES

134  
135

135 JULES is a process-based model that integrates water, energy, C cycling (JULES-C) (Clark *et al.*, 2011) and N  
136 cycling (JULES-CN) (Wiltshire *et al.*, 2021) between the atmosphere, vegetation and soil (Best *et al.*, 2011;  
137 Clark *et al.*, 2011). Vegetation dynamics are represented in JULES using the TRIFFID model, using nine  
138 distinct plant functional types (PFTs) (tropical and temperate broadleaf evergreen trees, broadleaf deciduous  
139 trees, needle-leaf evergreen and deciduous trees, C3 and C4 grasses, and evergreen and deciduous shrubs), as  
140 well as height competition (Harper *et al.*, 2016). JULES simulates Gross Primary Productivity (GPP) based on a  
141 coupled photosynthesis and water balance scheme, from which autotrophic respiration for each living tissue  
142 (leaf, wood, root) is subtracted to estimate NPP. In JULES we assume a process-based leaf-level photosynthesis  
143 scaled up to the canopy. Therefore, in JULES CNP in order to keep consistency with JULES C-CN, we also  
144 assume a multi-level canopy, and leaf N and P in exponentially decreases through the canopy (CanRadMod 6)  
145 (Clark *et al.*, 2011). NPP is then allocated to increase tissue C stocks and to spread, i.e., expand the fractional  
146 coverage of the PFT. The resultant PFT fractional coverages depend in addition on competition across PFTs for  
147 resources, e.g., light. Tissue turnover and vegetation mortality add C into the litter pools. Representation of soil  
148 organic C (SOC) follows the RothC equations (Jenkinson *et al.*, 1990; Jenkinson and Coleman, 2008) defining  
149 four C pools: decomposable plant material (DPM) and resistant plant material (RPM), which receive direct input  
150 from litterfall, and microbial biomass (BIO) and humified material (HUM) which receive a fraction of  
151 decomposed C from DPM and RPM which is not released to the atmosphere. The limitation of N on SOC is  
152 applied to the vegetation and soil components using a dynamic C:N ratio to modify the mineralization and  
153 immobilization processes as described in Wiltshire *et al.*, (2021). Note that the soil component of JULES-CN  
154 can be run either as a single box model or vertically resolved over soil depth (JULES-CN layered), and in this  
155 paper we build upon the vertically resolved version described in Wiltshire *et al.* (2021).

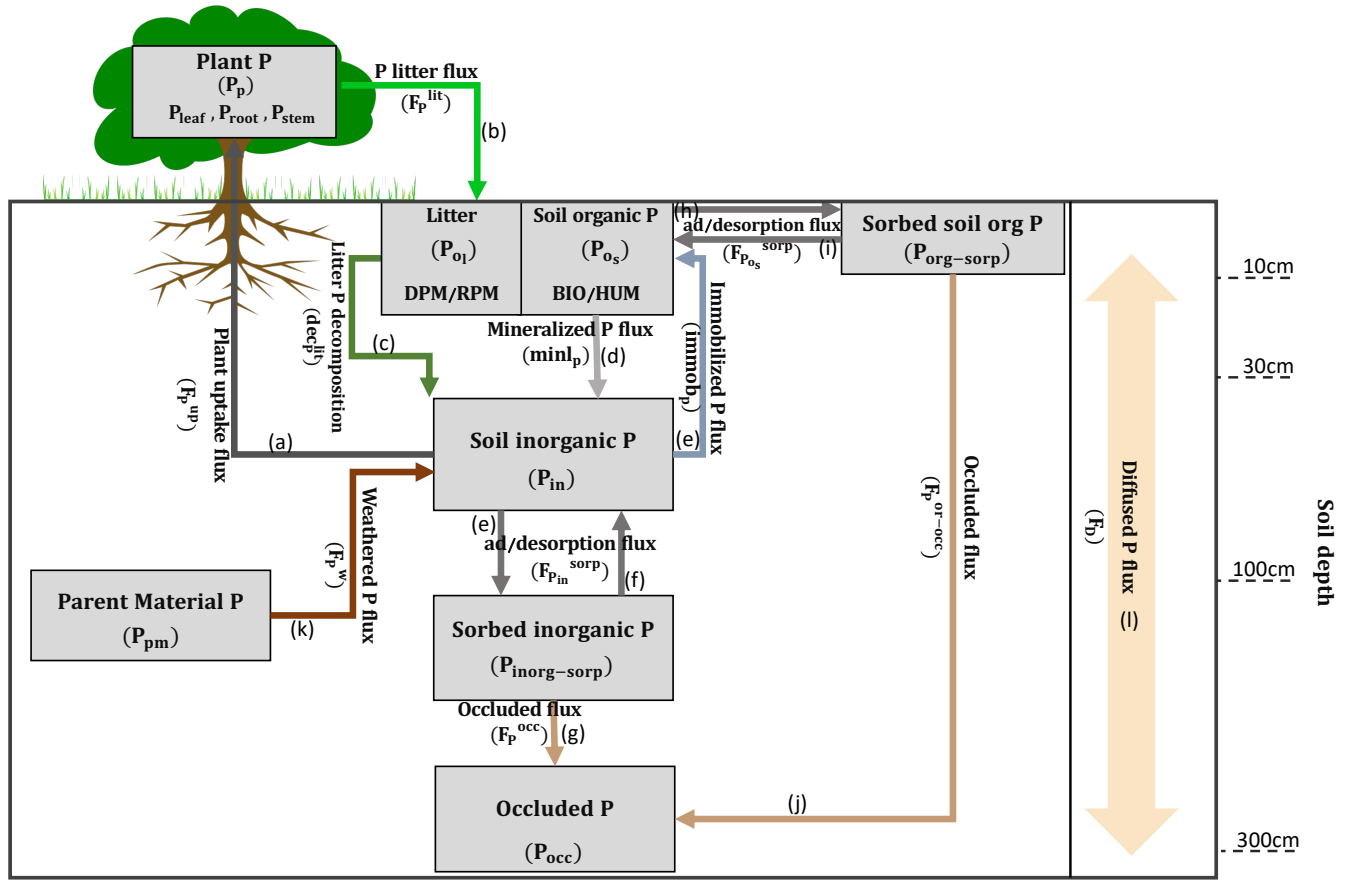
156  
157

### 157 2.2 JULES-CNP

158  
159

159 JULES-CNP includes the representation of the P cycle in JULES version (vn5.5). It includes P fluxes within the  
160 vegetation and soil components, and the specification of P pools and processes related to P cycling within the  
161 soil column (Figure.1). A parent material pool is introduced to consider the input of weathered P. The adsorbed,  
162 desorbed and occluded fractions of P for both organic and inorganic P are also represented. However, except for  
163 parent material and occluded P pools, all other pools are estimated at each soil layer. The description of changes

164 in pools and associated relative fluxes are explained in detail in the next sections. However, despite JULES-CN  
 165 that includes N leaching and deposition, P leaching and deposition are omitted in the current version of JULES-  
 166 CNP.  
 167  
 168



169  
 170 **Figure.1 – JULES CNP model scheme**

171  
 172 **2.2.1 P pools**

173  
 174 JULES represents eight P pools comprising organic and inorganic P: in plant P ( $P_p$ ) and soil pools (in each soil  
 175 layer (n)): litter P ( $P_{0l}$ ), soil organic P ( $P_{0s}$ ), soil inorganic P ( $P_{in}$ ), organic sorbed ( $P_{org-sorp}$ ), inorganic sorbed  
 176 ( $P_{inorg-sorp}$ ), parent material ( $P_{pm}$ ) and occluded ( $P_{occ}$ ) P comprised of both organic and inorganic P. All pools  
 177 are in units of  $\text{kg P m}^{-2}$  (Fig 1, Tables 1 and 2).  
 178

179 Plant P pool is composed of leaf ( $P_{leaf}$ ), fine root ( $P_{root}$ ) and stem together with coarse root ( $P_{stem}$ ), which are  
 180 related to their associated C pools ( $C_{leaf}, C_{root}, C_{stem}$ ) in ( $\text{kg C m}^{-2}$ ) and fixed C to P ratios  
 181 ( $C:P_{leaf}, C:P_{root}, C:P_{stem}$ ) as follows:  
 182

183 
$$P_{leaf} = \frac{C_{leaf}}{C:P_{leaf}} \quad (\text{eq.1})$$

184 
$$P_{root} = \frac{C_{root}}{C:P_{root}} \quad (\text{eq.2})$$

185 
$$P_{stem} = \frac{C_{stem}}{C:P_{stem}} \quad (\text{eq.3})$$

186  
 187  
 188 Therefore, the plant P pool ( $P_p$ ) is the sum of all vegetation P pools as follows:

189  
 190  
 191 
$$P_p = P_{leaf} + P_{root} + P_{stem} \quad (\text{eq.4})$$
  
 192

193 Description of the plant P pool ( $P_p$ ) follows Zhu *et al.*, (2016) and is estimated as the difference between the  
 194 input, plant uptake  $F_p^{up}$  (eq.26) and output of this pool, plant litter flux  $F_p^{lit}$  (eq.28), with both fluxes  
 195 expressed in kg P m<sup>-2</sup> yr<sup>-1</sup> as follows:

$$196 \frac{dP_p}{dt} = F_p^{up} - F_p^{lit} \quad (\text{eq.5})$$

197  
 198 The litter P pool ( $P_{ol}$ ) is estimated as a sum of  $P_{DPM}$  and  $P_{RPM}$  pools. Each pool is formed by the fluxes of plant  
 199 litter input ( $F_p^{lit}$ ) and the outgoing decomposed P ( $dec_p^{lit}$ ) both expressed in kg P m<sup>-2</sup> yr<sup>-1</sup> (eq.28-29).  
 200 Furthermore, the plant litter input is modified based on the plant type material ratio  $\alpha$  (in order to distribute the  
 201 litter input based on the DPM/RPM fraction) as follows:

$$202 \frac{dP_{DPM}}{dt} = F_{p_n}^{lit} \times \alpha - dec_{P_{DPM},n} \quad (\text{eq.6})$$

$$203 \frac{dP_{RPM}}{dt} = F_{p_n}^{lit} \times (1 - \alpha) - dec_{P_{RPM},n} \quad (\text{eq.7})$$

$$204 P_{ol} = \sum_{n=1}^N P_{DPM,n} + \sum_{n=1}^N P_{RPM,n} \quad (\text{eq.8})$$

205  
 206 The soil organic pool ( $P_{os}$ ) is represented as the sum of  $P_{BIO}$  and  $P_{HUM}$ . These pools are estimated from the  
 207 difference between P inputs from total immobilized ( $F_{immob_p}$ ) distributed between BIO and HUM based on  
 208 fixed fraction (0.46 for BIO, 0.54 for HUM) (Jenkinson *et al.*, 1990; Jenkinson and Coleman, 2008) and  
 209 desorbed P  $F_{P_{os}}^{desorp}$  and P outputs from mineralized ( $F_{minl_p}$ ), and adsorbed P fluxes ( $F_{P_{os}}^{sorp}$ ) (adsorption:  
 210 eq. 40 and desorption: eq.41) with all fluxes expressed in kg P m<sup>-2</sup> yr<sup>-1</sup> as follows:

$$211 \frac{dP_{BIO}}{dt} = 0.46 \times F_{immob_{P_n}} + F_{P_{os_{BIO},n}}^{desorp} - F_{minl_{P_{BIO},n}} - F_{P_{os_{BIO},n}}^{sorp} \quad (\text{eq.9})$$

$$212 \frac{dP_{HUM}}{dt} = 0.54 \times F_{immob_{P_n}} + F_{P_{os_{HUM},n}}^{desorp} - F_{minl_{P_{BIO},n}} - F_{P_{os_{HUM},n}}^{sorp} \quad (\text{eq.10})$$

$$213 P_{os} = \sum_{n=1}^N P_{BIO,n} + \sum_{n=1}^N P_{HUM,n} \quad (\text{eq.11})$$

214  
 215 Description of the inorganic sorbed P pool ( $P_{inorg-sorp}$ ) follows Wang *et al.*, (2007) and is represented as the  
 216 difference between the input flux of inorganic sorption ( $F_{p_{in}}^{sorp}$ ) (eq. 37) and output fluxes of inorganic  
 217 desorption ( $F_{p_{in}}^{desorp}$ ) (eq. 38) and occluded P ( $F_p^{occ}$ ) (eq. 39), with all fluxes expressed in kg P m<sup>-2</sup> yr<sup>-1</sup> as  
 218 follows:

$$219 \frac{dP_{inorg-sorp}}{dt} = \sum_{n=1}^N F_{p_{in},n}^{sorp} - \sum_{n=1}^N F_{p_{in},n}^{desorp} - \sum_{n=1}^N F_{p_n}^{occ} \quad (\text{eq.12})$$

220  
 221 Describing of the occluded ( $P_{occ}$ ) P pool follows Wang *et al.*, (2007) and Hou *et al.*, (2019) and is represented  
 222 as the sum of input fluxes of occluded P from both organic ( $F_p^{or-occ}$ ) (eq. 42) and inorganic P pools ( $F_p^{occ}$ )  
 223 expressed in kg P m<sup>-2</sup> yr<sup>-1</sup>, as follows:

$$224 \frac{dP_{occ}}{dt} = \sum_{n=1}^N F_{p_n}^{occ} + \sum_{n=1}^N F_{p_n}^{or-occ} \quad (\text{eq.13})$$

225  
 226 Describing of the organic sorbed P pool ( $P_{org-sorp}$ ) follows Wang *et al.*, (2007) and is represented as the  
 227 difference between the input flux of organic sorption ( $F_{P_{os_n}}^{sorp}$ ) and output fluxes of organic desorption  
 228 ( $F_{P_{os_n}}^{desorp}$ ) and occluded P ( $F_{p_n}^{occ}$ ), with all fluxes expressed in kg P m<sup>-2</sup> yr<sup>-1</sup> as follows:

$$229 \frac{dP_{org-sorp}}{dt} = \sum_{n=1}^N F_{P_{os_n}}^{sorp} - \sum_{n=1}^N F_{P_{os_n}}^{desorp} - \sum_{n=1}^N F_{p_n}^{or-occ} \quad (\text{eq.14})$$

230  
 231  
 232  
 233  
 234  
 235  
 236  
 237  
 238  
 239  
 240  
 241  
 242  
 243

244 Describing of P from parent material ( $P_{pm}$ ) pool follows Wang *et al.*, (2007) and depends on the weathering  
 245 flux ( $F_p^w$ ) (eq. 43) in kg P m<sup>-2</sup> yr<sup>-1</sup> as follows:

$$247 \frac{dP_{pm}}{dt} = - \sum_{n=1}^N F_{P_n}^w \quad (\text{eq.15})$$

### 248 2.2.2. C and P fluxes

251 NPP in JULES is calculated as the difference between GPP and autotrophic respiration. In JULES-CNP,  
 252 potential NPP represent the amount of C, available for tissue growth (C density increase) on a unit area, and  
 253 spreading (vegetation cover increase as a result of reproduction and recruitment), ie to increase the area covered  
 254 by the vegetation type, assuming no nutrient limitation. The reported NPP in the literature often includes other C  
 255 fluxes related to the exudates, volatiles production and non-structural carbohydrates (Malhi *et al.*, 2009; Chapin  
 256 *et al.*, 2011; Walker *et al.*, 2021) which are challenging to measure (Malhi, Doughty and Galbraith, 2011).  
 257 Therefore, actual NPP is for our purposes equal to Biomass Production (BP), and is calculated as potential NPP  
 258 minus excess C (lost to the plant through autotrophic respiration), with the latter the C that cannot be used to  
 259 growth new plant tissue due to insufficient plant nutrient supply. Hence, if the system is limited by the  
 260 availability of N and/or P, NPP will be adjusted to match the growth that can be supported with the limited N or  
 261 P supply, with any excess carbohydrate lost through excess C.

262 The total excess C term ( $\psi_t$ ) (kg C m<sup>-2</sup> yr<sup>-1</sup>) is calculated as:

$$264 \psi_t = \psi_g + \psi_s \quad (\text{eq.16})$$

265 where  $\psi_g$  and  $\psi_s$  are the excess C fluxes due to growth (g) and spread (s) and are assumed to be rapidly respired  
 266 by plants.

269 Therefore, BP is calculated as the difference between potential NPP ( $\Pi_c$ ) and total excess C:

$$271 BP = \Pi_c - \psi_t \quad (\text{eq.17})$$

273 The litter production in JULES before limitation is estimated based on the as follows:

$$275 F_{C_n}^{lit} = \gamma_{leaf} C_{leaf} + \gamma_{root} C_{root} + \gamma_{wood} C_{wood} \quad (\text{eq.18})$$

277 where  $\lambda$  is the leaf, root and stem re-translocation (at daily timestep) coefficient (Clark *et al.*, 2011) and  $\gamma$  is a  
 278 temperature dependent turnover rate representing the phenological state (Clark *et al.*, 2011). P limitation is  
 279 applied on the C litter production similar to the N scheme of JULES (JULES-CN) (Wiltshire *et al.*, 2021). In  
 280 JULES-CN the N limitation effect on the litter production is captured by estimating the available C for litter  
 281 production as a difference between the NPP and excess C (Wiltshire *et al.*, 2021).

283 Similar to other P-enabled models (Yang *et al.*, 2014; Goll *et al.*, 2017), JULES-CNP follows the same structure  
 284 as its N model component. Description of the plant P and N demand follow Wang *et al.*, (2007) and are  
 285 represented by the sum of demand ( $\phi_t$ ) to sustain growth (P-related: ( $\phi_{gP}$ ), N-related: ( $\phi_{gN}$ )) and to sustain  
 286 vegetation spreading (to increment PFT fractional coverage) (P-related: ( $\phi_{sP}$ ), N-related: ( $\phi_{sN}$ )) and is  
 287 expressed in (P-related in kg P m<sup>-2</sup> yr<sup>-1</sup>; N-related in kg N m<sup>-2</sup> yr<sup>-1</sup>). The total demand for growth ( $\phi_g$ ) and  
 288 spreading ( $\phi_s$ ) is controlled by the dominant demand between P ( $\phi_{gP}$ ) and N ( $\phi_{gN}$ ) as follows:

$$290 \phi_t = \phi_g + \phi_s \quad (\text{eq.19})$$

$$291 \phi_{gP} = \frac{P_p}{C_v} \left( \Pi_c - \frac{dC_v}{dt} - \psi_g \right) \quad (\text{eq.20})$$

$$292 \phi_{sP} = \frac{P_p}{C_v} \left( \Pi_c - \frac{dC_v}{dt} - \psi_s \right) \quad (\text{eq.21})$$

$$293 \phi_{gN} = \frac{N_v}{C_v} \left( \Pi_c - \frac{dC_v}{dt} - \psi_g \right) \quad (\text{eq.22})$$

$$294 \phi_{sN} = \frac{N_v}{C_v} \left( \Pi_c - \frac{dC_v}{dt} - \psi_s \right) \quad (\text{eq.23})$$

$$295 \phi_g = \begin{cases} \phi_{gP} & \phi_{gP} \times \frac{C_v}{P_p} > \phi_{gN} \times \frac{C_v}{N_v} \\ \phi_{gN} & \phi_{gN} \times \frac{C_v}{N_v} > \phi_{gP} \times \frac{C_v}{P_p} \end{cases} \quad (\text{eq.24})$$



$$\phi_s = \begin{cases} \phi_{sP} & \phi_{sP} \times \frac{C_V}{P_p} > \phi_{sN} \times \frac{C_V}{N_v} \\ \phi_{sN} & \phi_{sN} \times \frac{C_V}{N_v} > \phi_{sP} \times \frac{C_V}{P_p} \end{cases} \quad (\text{eq.25})$$

297  
298

299 where  $\frac{P_p}{C_V}$  is the inverse of whole plant C:P ratio,  $\frac{N_v}{C_V}$  is inverse plant C:N ratio,  $\frac{dC_V}{dt}$  is rate of change in plant C  
300 (see Clark *et al.*, (2011) for more detail),  $\Pi_c$  is nutrient-unlimited, or potential, NPP (kg C m<sup>-2</sup> yr<sup>-1</sup>),  $\psi_g$  is excess  
301 C due to either P or N limitation for plant growth (kg C m<sup>-2</sup> yr<sup>-1</sup>) and  $\psi_s$  is excess C due to either P or N  
302 limitation for vegetation spreading (kg C m<sup>-2</sup> yr<sup>-1</sup>).  
303

304 Equations 20 and 22 are solved by first setting  $\psi_g = 0.0$  to find the total plant P (eq. 20) and N demand (eq.22).  
305 If the P and N demand for growth are less than the available P and N and fractional coverage ( $\lambda$ ) (NPP fraction  
306 used for fractional cover increment; for detail see Wiltshire *et al.*, (2021)) at the considered timestep  $\Delta t$  then  
307 there is no limitation to growth (*i. e.*  $\phi_{gP} < \frac{(1-\lambda)P_{avail}}{\Delta t}$ ;  $\phi_{gN} < \frac{(1-\lambda)N_{avail}}{\Delta t}$ ). Where there is limited P and/or N  
308 availability, the uptake equals the available P and N ( $\phi_{gP} = \frac{(1-\lambda)P_{avail}}{\Delta t}$ ;  $\phi_{gN} = \frac{(1-\lambda)N_{avail}}{\Delta t}$ ), and the plant  
309 growth which cannot be achieved due to nutrient constraints will be deducted from potential NPP, here termed  
310 excess C term ( $\psi_g$ ), to give an actual NPP. Following Wiltshire *et al.*, 2021, we assume excess C is respired by  
311 the plant.

312 Similarly, in order to estimate the P and N demand for spreading (eq. 21 and 23), initially the excess C from  
313 spreading is set to 0.0 ( $\psi_s = 0.0$ ), *i.e.* under the assumption that there is no nutrient limitation. If the P and N  
314 demand for spreading are lower than the available P and N and fractional coverage ( $\lambda$ ) ( $\phi_{sP} <$   
315  $\frac{(1-\lambda)P_{avail}}{\Delta t}$ ;  $\phi_{sN} < \frac{(1-\lambda)N_{avail}}{\Delta t}$ ), then there is no limitation on spreading and in case of limited P and N  
316 availability, the uptake equals the available P and N ( $\phi_{sP} = \frac{(1-\lambda)P_{avail}}{\Delta t}$ ;  $\phi_{sN} = \frac{(1-\lambda)N_{avail}}{\Delta t}$ ), and the excess C  
317 for spread ( $\psi_s$ ) is subtracted from potential NPP.  
318

319 Plant P uptake ( $F_p^{up}$ ) (arrow a in Fig 1) is estimated based on the P demand for growth and spreading ( $\phi_t$ ) and  
320 the root uptake capacity ( $u^{max}$ ) (kg P kg<sup>-1</sup> C yr<sup>-1</sup>), as follows:  
321

$$F_p^{up} = \begin{cases} \phi_t & \phi_t \leq u^{max} \\ u^{max} & \phi_t > u^{max} \end{cases} \quad (\text{eq.26})$$

323

324 Description of the plant P uptake ( $F_p^{up}$ ) varies spatially depending on the root uptake capacity ( $u^{max}$ ) followed  
325 by Goll *et al.*, (2017). Therefore, in regions with limited P supply, the plant P uptake is limited to the  $u^{max}$  and  
326 consequently impacts the excess C and BP.

327 The root uptake capacity depends on the maximum root uptake capacity ( $v_{max}$ ) (kg P kg<sup>-1</sup> C yr<sup>-1</sup>), root depth  
328 ( $d_{root}$ ), the concentration of inorganic p at different soil depths ( $P_{in}$ ), and a half saturation term at which half of  
329 the maximum uptake capacity is reached using inorganic p at different soil depths ( $P_{in}$ ), a scaling uptake ratio  
330 ( $K_p$ ) ( $\mu\text{mol P l}^{-1}$ ), unit conversion ( $C_f$ ) (1 kg P<sup>-1</sup>), and soil moisture ( $\theta$ ) (1 m<sup>-2</sup>), as follows:  
331

$$u^{max} = v_{max} \times d_{root} \times \sum_{n=1}^N P_{in_n} \times \left( \frac{1}{\sum_{n=1}^N P_{in_n} + c_f \times K_p \times \theta_n} \right) \quad (\text{eq.27})$$

333

334 Description of the litter production of P ( $F_{P_n}^{lit}$ ) (arrow b in Fig 1) follows JULES-CN as in Wiltshire *et al.*,  
335 (2021) and is calculated based on the litter flux of C (kg C m<sup>-2</sup> yr<sup>-1</sup>) using leaf, root and wood turnovers (yr<sup>-1</sup>),  
336 and through the vegetation dynamics due to large-scale disturbance and litter production density, as follows:  
337

$$F_{P_n}^{lit} = (1 - k_{leaf})\gamma_{leaf}C_{leaf} \times C:P_{leaf} + (1 - k_{root})\gamma_{root}C_{root} \times C:P_{root} + \gamma_{wood}C_{wood} \times C:P_{stem} \quad (\text{eq.28})$$

339

340 where  $\lambda$  is the leaf, root and stem re-translocation (at daily timestep) coefficient (Zaehle and Friend, 2010; Clark  
341 *et al.*, 2011) and the related C:P ratios for P fraction and  $\gamma$  is a temperature dependent turnover rate representing  
342 the phenological state (Clark *et al.*, 2011).  
343  
344  
345

346 The decomposition of litter ( $dec^{lit}$ ) (arrow c in Fig 1) depends on soil respiration ( $R$ ) (kg C m<sup>-2</sup> yr<sup>-1</sup>), the litter  
 347 C:P ratio ( $C:P_{lit}$ ) at each soil layer ( $n$ ) as follows:

$$348 \quad 349 \quad dec_p^{lit} = \frac{\sum_{n=1}^N R_n}{C:P_{lit}} \quad (eq.29)$$

350 where the  $C:P_{lit}$  is calculated based on litter C pool (DPM and RPM) ( $lit^C$ ) (kg C m<sup>-2</sup> yr<sup>-1</sup>) and litter P pool  
 351 ( $P_{O_i}$ ) as follows:

$$352 \quad 353 \quad 354 \quad C:P_{lit} = \frac{\sum_{n=1}^N lit_n^C}{P_{O_{i_n}}} \quad (eq.30)$$

355 The mineralized ( $F_{minl_p}$ ) (arrow d in Fig 1) and immobilized ( $F_{immob_p}$ ) (arrow e in Fig 1) P fluxes are  
 356 calculated based on C mineralization and immobilization, C:P ratios of plant (i) (DPM/RPM) ( $C:P_{plant}$ ) and  
 357 soil (HUM/BIO) ( $C:P_{soil}$ ), soil pool potential respiration ( $R_{POT_i}$ ) (kg C m<sup>-2</sup> yr<sup>-1</sup>) and the respiration partitioning  
 358 fraction ( $resp\_frac$ ) as follows:

$$359 \quad 360 \quad 361 \quad F_{minl_{p_n}} = \frac{\sum_{n=1}^N R_{POT_{i_n}}}{\epsilon_{cp_i}} \quad (eq.31)$$

$$362 \quad 363 \quad F_{immob_{p_n}} = \frac{\sum_{n=1}^N R_{i_n} \times resp\_frac}{C:P_{soil}} \quad (eq.32)$$

364 The soil respiration from each soil layer ( $R_{i_n}$ ) is estimated from potential soil respiration ( $R_{POT_{i_n}}$ ) for the  
 365 DPM, RPM pools and the litter decomposition rate modifier ( $F_{P_n}$ ) as follows:

$$366 \quad 367 \quad 368 \quad R_{i_n} = R_{POT_{i_n}} \times F_{P_n} \quad (eq.33)$$

369 where the description of  $F_{P_n}$  for P pools ( $F_{P_{P_n}}$ ) follows Wang *et al.*, (2007) and is estimated based on the soil  
 370 pool (BIO/HUM) mineralization ( $minl_{p-BIO_n}$ ,  $minl_{p-HUM_n}$ ) and immobilization ( $immob_{p-BIO_n}$ ,  
 371  $immob_{p-HUM_n}$ ) (in kg P m<sup>-2</sup> yr<sup>-1</sup>), soil inorganic P ( $P_{inorg_n}$ ) (in kg P m<sup>-2</sup>), and litter pools (DPM/RPM) demand  
 372 (in kg P m<sup>-2</sup> yr<sup>-1</sup>) as follows:

$$373 \quad 374 \quad 375 \quad F_{P_{P_n}} = \frac{(minl_{p-BIO_n} + minl_{p-HUM_n} - immob_{p-BIO_n} - immob_{p-HUM_n}) + P_{inorg_n}}{DEM_{DPM_n} + DEM_{RPM_n}} \quad (eq.34)$$

376 The net demand associated with decomposition of litter pools ( $DEM_{k,n}$ ) represents the P required by microbes  
 377 which convert DPM and RPM into BIO and HUM. The limitation due to insufficient P availability is estimated  
 378 based on the potential mineralization ( $minl_{p-pot}$ ) and immobilization ( $immob_{p-pot}$ ) (in kg P m<sup>-2</sup> yr<sup>-1</sup>) of pools  
 379 (k) as follows:

$$380 \quad 381 \quad 382 \quad DEM_{k,n} = immob_{p-pot,k} - minl_{p-pot,k} \quad (eq.35)$$

383 The  $F_{P_n}$  estimated for N pools ( $F_{P_{N_n}}$ ) follows the same formulation as P (see Wiltshire *et al.*, 2021 for detail)  
 384 and the  $F_{P_n}$  is estimated based on a higher rate modifier between N and P as follows:

$$385 \quad 386 \quad 387 \quad F_{P_n} = \begin{cases} F_{P_{P_n}} & F_{P_{P_n}} > F_{P_{N_n}} \\ F_{P_{N_n}} & F_{P_{N_n}} > F_{P_{P_n}} \end{cases} \quad (eq.36)$$

388 Description of the fluxes of adsorption ( $F_{P_{in_n}^{sorp}}$ ) (arrow e in Fig 1) and desorption ( $F_{P_{in_n}^{desorp}}$ ) (arrow f in Fig  
 389 1) of inorganic P in kg P m<sup>-2</sup> yr<sup>-1</sup> follow Wang *et al.*, (2010) and are calculated based on soil inorganic ( $P_{in_n}$ ) and  
 390 sorbed inorganic ( $P_{inorg-sorbed_n}$ ) P pools and inorganic adsorption ( $K_{sorp-in}$ ), desorption ( $K_{desorp-in}$ )  
 391 coefficients (kg P m<sup>-2</sup> yr<sup>-1</sup>) and maximum sorbed inorganic ( $P_{in-max}$ ) (kg P m<sup>-2</sup>) as follows:

$$392 \quad 393 \quad 394 \quad F_{P_{in_n}^{sorp}} = P_{in_n} \times K_{sorp-in} \times \frac{(P_{in-max_n} - P_{inorg-sorbed_n})}{P_{in-max_n}} \quad (eq.37)$$



395  
 396  $F_{P_{in_n}}^{desorp} = P_{inorg-sorbed_n} \times K_{desorp-in}$  (eq.38)  
 397

398 Description of the occluded inorganic P flux ( $F_{P_n}^{occ}$ ) (arrow g in Fig 1) follows Wang *et al.*, (2007) and Hou *et*  
 399 *al.*, (2019) and is calculated based on sorbed inorganic P pool and P occlusion rate ( $K_{occ}$ ) ( $\text{kg P m}^{-2} \text{ yr}^{-1}$ ) as  
 400 follows:

401  
 402  $F_{P_n}^{occ} = P_{inorg-sorbed_n} \times K_{occ}$  (eq.39)  
 403

404 Description of the fluxes of adsorption ( $F_{P_{O_{S_n}}}^{sorp}$ ) (arrow h in Fig 1) and desorption ( $F_{P_{O_{S_n}}}^{desorp}$ ) (arrow i in Fig  
 405 1) of organic P follow Wang *et al.*, (2010) are calculated based on soil organic and sorbed organic P pools and  
 406 organic adsorption ( $K_{sorp-or}$ ) ( $\text{kg P m}^{-2} \text{ yr}^{-1}$ ), desorption ( $K_{desorp-or}$ ) coefficients ( $\text{kg P m}^{-2} \text{ yr}^{-1}$ ) and maximum  
 407 sorbed organic ( $P_{org-max}$ ) (which corresponds to the sorbed soil P saturation, thus modifying the sorption rate  
 408 respectively) ( $\text{kg P m}^{-2}$ ) as follows:  
 409

410  $F_{P_{O_{S_n}}}^{sorp} = P_{O_{S_n}} \times K_{sorp-or} \times \frac{(P_{or-max_n} - P_{org-sorbed_n})}{P_{or-max_n}}$  (eq.40)  
 411

412  $F_{P_{O_{S_n}}}^{desorp} = P_{org-sorbed_n} \times K_{desorp-or}$  (eq.41)  
 413

414 Description of the occluded organic P flux ( $F_{P_n}^{or-occ}$ ) ( $\text{kg P m}^{-2} \text{ yr}^{-1}$ ) (arrow j in Fig 1) follows Wang *et al.*,  
 415 (2007) and Hou *et al.*, (2019) is calculated based on sorbed organic P pool ( $P_{org-sorbed_n}$ ) and P occlude rate  
 416 ( $K_{occ}$ ) ( $\text{kg P m}^{-2} \text{ yr}^{-1}$ ) as follows:  
 417

418  $F_{P_n}^{or-occ} = P_{org-sorbed_n} \times K_{occ}$  (eq.42)  
 419

420 Description of the P flux from weathered parent material ( $F_{P_n}^w$ ) (arrow k in Fig 1) follows Wang *et al.*, (2007)  
 421 and is calculated based on amount of P in the parent material ( $P_{pm}$ ) and P weathering rate ( $K_w$ ) ( $\text{kg P m}^{-2} \text{ yr}^{-1}$ ) as  
 422 follows:  
 423

424  $F_{P_n}^w = P_{pm_n} \times K_w$  (eq.43)  
 425

426 Description of P diffusion between soil layers ( $F_{D_n}$ ) expressed in ( $\text{kg P m}^{-2} \text{ yr}^{-1}$ ) (arrow l in Fig 1) follows Goll  
 427 *et al.*, (2017) and is calculated following Fick's second law and it is a function of the diffusion coefficient ( $Dz$ )  
 428 in  $\text{m}^2 \text{ s}^{-1}$ , the concentration of inorganic P at different soil depths ( $P_{in}$ ) in  $\text{kg P m}^{-2}$ , the distance ( $z$ ) between the  
 429 midpoints of soil layers in metres and seconds to year unit conversion ( $Yr$ ):  
 430

431  $F_{D_n} = \frac{\partial}{\partial z} (D_{z_n} \frac{\partial P_{S_n}}{\partial z}) \times Yr$  (eq.44)  
 432  
 433  
 434  
 435  
 436  
 437  
 438  
 439  
 440  
 441  
 442  
 443  
 444  
 445  
 446

447 **Table 1.** Model variables

<b>Variable</b>	<b>Unit</b>	<b>Definition</b>
$\Psi$	kg C m <sup>-2</sup> yr <sup>-1</sup>	Excess C flux
$\emptyset$	kg P m <sup>-2</sup> yr <sup>-1</sup>	Plant demand for uptake
$\Pi_c$	kg C m <sup>-2</sup> yr <sup>-1</sup>	Potential NPP
$u^{max}$	kg P kg <sup>-1</sup> C yr <sup>-1</sup>	Root uptake capacity
$DEM$	kg P m <sup>-2</sup> yr <sup>-1</sup>	Plant pool P associated decomposition demand
$dec_P^{lit}$	kg P m <sup>-2</sup> yr <sup>-1</sup>	Litter decomposition
$F_D$	kg P m <sup>-2</sup> yr <sup>-1</sup>	Plant diffusion flux
$F_P$	-	Plant litter decomposition rate modifier
$F_P^{lit}$	kg P m <sup>-2</sup> yr <sup>-1</sup>	Plant litter flux
$F_P^{up}$	kg P m <sup>-2</sup> yr <sup>-1</sup>	Plant uptake
$F_{PO_S}^{sorp}$	kg P m <sup>-2</sup> yr <sup>-1</sup>	Sorbed organic P flux
$F_{P_{in}}^{sorp}$	kg P m <sup>-2</sup> yr <sup>-1</sup>	Sorbed inorganic P flux
$F_{PO_S}^{desorp}$	kg P m <sup>-2</sup> yr <sup>-1</sup>	Desorbed organic P flux
$F_{P_{in}}^{desorp}$	kg P m <sup>-2</sup> yr <sup>-1</sup>	Desorbed inorganic P flux
$F_P^{occ}$	kg P m <sup>-2</sup> yr <sup>-1</sup>	Occluded inorganic P flux
$F_P^{or-occ}$	kg P m <sup>-2</sup> yr <sup>-1</sup>	Occluded organic P flux
$F_P^w$	kg P m <sup>-2</sup> yr <sup>-1</sup>	Weathered P flux
$F_{immob_P}$	kg P m <sup>-2</sup> yr <sup>-1</sup>	Immobilized P flux
$lit_C$	kg C m <sup>-2</sup> yr <sup>-1</sup>	C litter flux
$lit_{frac}$	-	Litter fraction
$lit_{leaf}$	kg C m <sup>-2</sup> yr <sup>-1</sup>	Leaf litter flux
$lit_{root}$	kg C m <sup>-2</sup> yr <sup>-1</sup>	Root litter flux
$lit_{wood}$	kg C m <sup>-2</sup> yr <sup>-1</sup>	Woody litter flux
$F_{minl_P}$	kg P m <sup>-2</sup> yr <sup>-1</sup>	Mineralized P flux
$P_p$	kg P m <sup>-2</sup>	Plant P pool
$P_{O_l}$	kg P m <sup>-2</sup>	Litter organic pool
$P_{O_S}$	kg P m <sup>-2</sup>	Soil organic pool
$P_{in}$	kg P m <sup>-2</sup>	Soil inorganic pool
$P_{inorg-sorp}$	kg P m <sup>-2</sup>	Soil inorganic sorbed pool
$P_{org-sorp}$	kg P m <sup>-2</sup>	Soil organic sorbed pool
$P_{occ}$	kg P m <sup>-2</sup>	Soil occluded pool
$P_{pm}$	kg P m <sup>-2</sup>	Parent material pool
$R$	kg C m <sup>-2</sup> yr <sup>-1</sup>	Total respiration
$R_{POT}$	kg C m <sup>-2</sup> yr <sup>-1</sup>	Total potential respiration
$R^S$	kg C m <sup>-2</sup> yr <sup>-1</sup>	Soil respiration
$R_d$	kg C m <sup>-2</sup> yr <sup>-1</sup>	Leaf dark respiration
$T_{ref}$	K	Soil reference temperature
$T_s$	K	Soil temperature
$Veg_c$	kg C m <sup>-2</sup>	Sum of biomass
$z$	m	Soil depth

448  
449  
450  
451  
452  
453

454  
455

**Table 2.** P Model parameters

Parameter	Value	Unit	Eq.	Description	Source
<b>C and N related</b>					
$\alpha$	0.25	-	6	Plant type material ratio	(Clark <i>et al.</i> , 2011)
$a_{wl}$	1.204	kg C m <sup>-2</sup>	50	Allometric coefficient	calibrated
$\sigma_l$	0.0375	kg C m <sup>-2</sup> per unit LAI	48	Specific leaf density	Clark <i>et al.</i> , 2011
$b_{wl}$	1.667	-	50	Allometric exponent.	Clark <i>et al.</i> , 2011
$f_{dr}$	0.005	-	47	Respiration scale factor	Calibrated
$resp\_frac$	0.25	-	32	Respiration fraction	(Clark <i>et al.</i> , 2011)
$k_{leaf}$	0.5	-	28	Leaf N re-translocation coefficient	(Zachle and Friend, 2010)
$k_{root}$	0.2	-	28	Root N re-translocation coefficient	(Zachle and Friend, 2010)
$d_{root}$	3.0	-	27	Root fraction in each soil layer	(Clark <i>et al.</i> , 2011)
$v_{int}$	7.21	$\mu\text{mol CO}_2 \text{ m}^{-2} \text{ s}^{-1}$	45	Intercept in the linear regression between $V_{\text{cmax}}$ and $N_{\text{area}}$	Calibrated (Clark <i>et al.</i> , 2011)
$v_{sl}$	19.22	$\mu\text{mol CO}_2 \text{ gN}^{-1} \text{ s}^{-1}$	45	Slope in the linear regression between $V_{\text{cmax}}$ and $N_{\text{area}}$	Calibrated (Clark <i>et al.</i> , 2011)
$LMA$	131.571852	g m <sup>-2</sup>	45	Observed Leaf Mass per Area	Study site
$Leaf\ N$	1.79007596	g g <sup>-1</sup>	45, 46	Foliar N concentrations in area basis	Study site
<b>P related</b>					
$C:P_{soil}$	1299.6	-	32	Soil C:P ratio	(Fleischer <i>et al.</i> , 2019)
$v_{max}$	0.0007	kg P kg <sup>-1</sup> C yr <sup>-1</sup>	27	Maximum root uptake capacity	Calibrated (Goll <i>et al.</i> , 2017)
$P$	0.7083062	g kg <sup>-1</sup>	46	Foliar P concentrations	Study site
$c_f$	$3.1 \times 10^{-5}$	l kg P <sup>-1</sup>	27	Conversion factor	(Goll <i>et al.</i> , 2017)
$D_z$	0.001	m <sup>2</sup> s <sup>-1</sup>	44	Diffusion coefficient	(Burke <i>et al.</i> , 2017)
$K_{occ}$	$1.2 \times 10^{-5}$	yr <sup>-1</sup>	39, 42	P occlusion rate	(Yang <i>et al.</i> , 2014)
$K_p$	3.0	kg P l <sup>-1</sup>	27	Scaling uptake ratio	Calibrated
$K_{sorp-in}$	0.0054	kg P m <sup>-2</sup> yr <sup>-1</sup>	37	Inorganic P adsorption coefficient	Calibrated (Hou <i>et al.</i> , 2019)
$K_{sorp-or}$	0.00054	kg P m <sup>-2</sup> yr <sup>-1</sup>	40	Organic P adsorption coefficient	Calibrated
$K_{in-max}$	0.0075	kg P m <sup>-2</sup> yr <sup>-1</sup>	37	Maximum sorbed inorganic P	Study site
$K_{or-max}$	0.0042	kg P m <sup>-2</sup> yr <sup>-1</sup>	40	Maximum sorbed organic P	Study site
$K_w$	$3 \times 10^{-6}$	kg P m <sup>-2</sup> yr <sup>-1</sup>	43	P weathering rate	(Wang <i>et al.</i> , 2010)

456  
457  
458  
459  
460  
461  
462  
463  
464  
465  
466  
467  
468  
469  
470  
471  
472

### 2.3 Study sites

This study uses data from two nearby sites in Central Amazon in Manaus, Brazil. The main site from here on termed *study site* (2°35'21.08" S, 60°06'53.63" W) (Lugli *et al.*, 2020) is for model development and evaluation. The second site is the Manaus K34 flux site (2°36'32.67" S, 60°12'33.48" W) which provides meteorological station data for running the model but also provides data for model evaluation. Our study site is the main lowland tropical forest site maintained by the National Institute for Amazon Research (INPA). Research at this site focuses on pre-experimental, plot, and full-scale long-term projects, combining experimental approaches (Keller *et al.*, 2004; Malhi *et al.*, 2009) with modelling (Lapola and Norby, 2014). Moreover, a recent manipulation experiment at this site provides an opportunity for future model testing under P fertilization. We use detailed novel soil and plant P pool data from the *study site* (Lugli *et al.*, 2020, 2021) for model parameterisation and calibration and carbon stock data for model validation. The *study site* has a very similar forest, geomorphology, soil chemistry and species composition to the well-known and studied K34 eddy covariance flux site (Araújo *et al.*, 2002). The average reported annual precipitation is 2431 (mm yr<sup>-1</sup>), with a monthly range of 95 to 304 (mm month<sup>-1</sup>), and averaged temperature is 26°C (Araújo *et al.*, 2002). Moreover, the soil class at this site is Geric Ferrosol with a high clay content and weathering activities (Malhi *et al.*, 2004).

473  
474  
475  
476  
477  
478  
479  
480  
481  
482  
483  
484  
485  
486  
487  
488  
489  
490  
491  
492  
493  
494  
495  
496  
497  
498  
499  
500  
501  
502  
503  
504  
505  
506  
507  
508  
509  
510  
511  
512  
513  
514  
515  
516  
517  
518  
519  
520  
521  
522  
523  
524  
525  
526  
527  
528  
529  
530  
531

## 2.4 Model parameterisation, calibration and evaluation

We use observations from the four control plots of the study site to parameterise, calibrate and evaluate different processes in JULES (Table 3). The observations were collected at 4 soil depths and processed using the Hedley sequential fractionation (Hedley, Stewart and Chauhan, 1982; Quesada *et al.*, 2010). Observed Leaf Mass per Area (LMA) leaf N and leaf P estimated from fresh leaves were used as input parameters to JULES to estimate photosynthetic capacity and respiration parameters. JULES vn5.5 (JULES CN in this study) estimates  $V_{cmax}$  ( $\mu\text{mol m}^{-2} \text{s}^{-2}$ ) based on Kattge *et al.* (2009) using foliar N concentrations in area basis ( $n_{leaf}$ ), as follows:

$$V_{cmax} = v_{int} + v_{sl} * n_{leaf} \quad (\text{eq.45})$$

where  $v_{int}$  is the estimated intercept and  $v_{sl}$  is the slope of the linear regression derived for the  $V_{cmax}$  estimation. We incorporated an additional P dependency on the estimation of  $V_{cmax}$  following Walker *et al.* (2014) as follows:

$$\ln(V_{cmax}) = 3.946 + 0.921 \ln(N) + 0.121 \ln(P) + 0.282 \ln(N) \ln(P) \quad (\text{eq.46})$$

Where N and P are foliar concentrations in area basis.

Implementation of eq. 46 resulted in higher  $V_{cmax}$  than in the original version of JULES. A higher  $V_{cmax}$  predicted higher leaf and plant respiration (eq.47). Constrained by observations of NPP and plant respiration at the study site, we modified one of the most uncertain parameters in the description of plant respiration ( $f_{dr}$ ) (eq.47) which is the scale factor ( $f_{dr}$ ) for leaf dark respiration ( $R_d$ ) as follows:

$$R_d = f_{dr} V_{cmax} \quad (\text{eq.47})$$

The default value for this scale factor is 0.01 (Clark *et al.*, 2011), and for JULES-CNP simulations at our study site it was modified to 0.005.

Observations of aboveground biomass were used to calibrate the non PFT dependent allometric relationships in JULES (Clark *et al.* 2011) (eq 48-50) for leaf, root and stem C. Specifically, the  $a_{wl}$  parameter (eq 50) was modified from 0.65 to 1.204 to match better tropical forest allometry:

$$C_{leaf} = \sigma_l L_b \quad (\text{eq.48})$$

$$C_{root} = C_{leaf} \quad (\text{eq.49})$$

$$C_{stem} = a_{wl} L_b^{b_{wl}} \quad (\text{eq.50})$$

Where  $\sigma_l$  is specific leaf density ( $\text{kg C m}^{-2}$  per unit LAI),  $L_b$  is balanced (or seasonal maximum) leaf area index ( $\text{m}^2 \text{m}^{-2}$ ),  $a_{wl}$  is allometric coefficient ( $\text{kg C m}^{-2}$ ) and  $b_{wl}$  is allometric exponent.

Note that JULES CNP uses C3 and C4 photosynthesis model from Collatz *et al.*, 1991; Collatz, Ribas-Carbo and Berry, 1992, which does not include estimation of  $J_{max}$ .

JULES-CNP has fixed stoichiometry and C:P ratios of leaf and root (measured), and wood (estimated from fresh coarse wood (Lugli, 2013)) which were taken from the *study site* and prescribed in JULES to simulate P dynamics in the plant. The following belowground data were used to represent various soil P pools: Resin and bicarbonate inorganic P (inorganic P:  $P_{in}$ ), organic bicarbonate P (organic P:  $P_{OS}$ ), NaOH organic P (sorbed organic P:  $P_{org-sorp}$ ), NaOH inorganic P (sorbed inorganic P:  $P_{inorg-sorp}$ ), residual P (occluded P:  $P_{occ}$ ) and HCL P (parent material P:  $P_{pm}$ ) (Table 3). The measurements were collected between 2017 and 2018 in control plots. All measurements were conducted at four soil layers (0-5, 5-10, 10-20, 20-30 cm). However, to be consistent with the JULES model soil layer discretization scheme, we defined 4 soil layers (0-10 cm, 10-30 cm, 30-100 cm and 100-300 cm) and we used the average between 0 and 30 cm to compare against the measurement from the same depth for model evaluation.

Vegetation C stocks were derived based on tree diameter measurements at breast height, that are linked to allometric equations and wood density databases to estimate the C stored in each individual tree, and then scaled to the plot (Chave *et al.*, 2014).

The organic and inorganic soil P assumed to be always at equilibrium with the relative sorbed pools (Wang, Law and Pak, 2010). Thus, in order to cap P sorption and uptake capacity, the maximum sorption capacities ( $P_{in-max_n}$ ,  $P_{or-max_n}$ , eq.37 and 39) (adopted from (Wang, Houlton and Field, 2007)) were prescribed using maximum observed sorbed inorganic and organic P. Hence, the maximum sorption capacity defines the

532 equilibrium state of sorbed and free-soil P. Moreover, as the magnitude of changes in the occluded and parent  
 533 material pools are insignificant over a short-term (20 years) simulation period (Vitousek *et al.*, 1997), these two  
 534 pools were prescribed using observations. Remaining parameters used to describe soil P fluxes (eq.s 27-44)  
 535 were prescribed using values from the literature (Table 3).

536  
 537 We used a combination of data from *Study site* and the nearby site K34 for model evaluation of C fluxes (GPP,  
 538 NPP) and C pools (soil and vegetation C, leaf, root and stem C) with no calibration on plant and soil organic and  
 539 soil inorganic P pools included (Table 3).

540  
 541 **Table 3.** Observations from study site (taken during 2017-2018) and from Manaus site K34 used for model parameterisation  
 542 and evaluation

Process	Variables	Purpose of use	Reference and site
C associated	GPP	Evaluation	Fleischer et al., 2019, K34
	NPP	Evaluation	Fleischer et al., 2019, K34
	Soil C	Evaluation	Malhi et al., 2009, K34
	CUE	Evaluation	Malhi et al., 2009, K34
	Veg C	Evaluation	Study site
	Leaf C	Evaluation	Study site
	Stem C	Evaluation	Study site
	Root C	Evaluation	Study site
	LAI	Initialisation	Study site
	LMA	Parameterisation	Study site
P associated	Resin	Evaluation	Study site
	Pi Bic	Evaluation	Study site
	Po Bic	Evaluation	Study site
	Po NaOH	Calibration	Study site
	Pi NaOH	Calibration	Study site
	P residual	Parameterisation	Study site
	P HCL	Parameterisation	Study site
	Leaf N	Parameterisation	Study site
	Leaf P	Parameterisation	Study site
	Root P	Parameterisation	Study site
Plant C:P ratio	Parameterisation	Study site	

543  
 544 **2.5 JULES simulations**  
 545

546 JULES was applied at the K34 flux tower site using observed meteorological forcing data from 1999-2019  
 547 (Fleischer et a 2019) at half hourly resolution. The following meteorological variables are needed to drive JULES  
 548 (model inputs) (Best *et al.*, 2011): atmospheric specific humidity ( $\text{kg kg}^{-1}$ ), atmospheric temperature (K), air  
 549 pressure at the surface (Pa), short and longwave radiation at the surface ( $\text{W m}^{-2}$ ), wind speed ( $\text{m s}^{-1}$ ) and total  
 550 precipitation ( $\text{kg m}^{-2} \text{s}^{-1}$ ). Furthermore, the averaged measured LAI from study site was used to initialise the  
 551 vegetation phenology module, but was allowed to vary in subsequent prognostic calculations. Soil organic and  
 552 inorganic sorbed P pools were initialised with study site observations. The JULES CNP simulations were  
 553 initialized following the same methodology as in Fleischer et al., (2019), by the spin-up from 1850 recycling  
 554 climatology to reach equilibrium state (Figure S1) and spin up was performed separately for three versions of  
 555 JULES (C/CN/CNP) following the same procedure. Furthermore, the transient run was performed for the period  
 556 1851-1998 using time-varying  $\text{CO}_2$  and N deposition fields. Finally, for the extended simulation period (1999-  
 557 2019) two runs were performed, the first with ambient the second elevated  $\text{CO}_2$  concentrations.

558  
 559 We evaluate the impact of including a P cycle in JULES using three model configurations (JULES C, CN and  
 560 CNP). We apply JULES in all three configurations using present day climate under both ambient  $\text{CO}_2$  and  
 561 elevated  $\text{CO}_2$  (e $\text{CO}_2$ ). Ambient and e $\text{CO}_2$  were prescribed following Fleischer *et al.*, (2019), with present-day  
 562  $\text{CO}_2$  based on global monitoring stations, and an abrupt (step) increase in atmospheric  $\text{CO}_2$  of +200 ppm on the  
 563 onset of the transient period (i.e., 1999). However, the comparison period is limited to 2017-18 for which the P  
 564 measurements are available.

565 We compare simulated C fluxes (GPP, NPP, litterfall C), C stocks (total vegetation, fine root, leaf, wood, soil)  
 566 and the  $\text{CO}_2$  fertilization effect across model configurations. The  $\text{CO}_2$  fertilization effect ( $\text{CO}_{2\text{fert-eff}}$ ) (eq.51)  
 567 is calculated based on simulated vegetation C under ambient ( $\text{VegC}(\text{aCO}_2)$ ) and e $\text{CO}_2$  ( $\text{VegC}(\text{eCO}_2)$ ) as  
 568 follows:

569

$$570 \quad CO2_{fert-eff} = \frac{(VegC(eCO_2) - VegC(aCO_2)) \times 100}{VegC(aCO_2)} \quad (eq.51)$$

571

572 Furthermore, the net biomass increases due to CO<sub>2</sub> fertilization effect ( $\Delta C_{veg}$ ) is estimated as follows:

573

$$574 \quad \Delta C_{veg} = \Delta BP - \Delta litterfall C \quad (eq.52)$$

575

576 We studied the Water Use Efficiency (WUE) (eq. 53) at half-hourly timestep, then aggregated per month as one  
577 of the main indicators of GPP changes (Xiao *et al.*, 2013), and soil moisture content (SMCL), as one of the  
578 main controllers of maximum uptake capacity (eq. 27), in order to better understanding the changes in GPP, P  
579 demand and uptake as well as excess C fluxes.

580

$$581 \quad WUE = GPP / Transpiration \quad (eq.53)$$

582

583 Moreover, we also estimated the Carbon Use Efficiency (CUE) as an indicator of the required C for the growth  
584 (Bradford and Crowther, 2013) as follows:

585

$$586 \quad CUE = BP / GPP \quad (eq.54)$$

587

588 We use JULES-CNP to evaluate the extent of P limitation under ambient and eCO<sub>2</sub> at this rainforest site in  
589 Central Amazon. P limitation is represented by the amount of C that is not used to grow new plant tissue due to  
590 insufficient P in the system (excess C) (eq. 27). The excess C flux is highly dependent on the plant P and the  
591 overall P availability to satisfy demand. We also explore the distribution of the inorganic and organic soil P and  
592 their sorbed fraction within the soil layer and under ambient and eCO<sub>2</sub>.

593

594 To test the sensitivity of the P and C related processes to the model P parameters, six sets of simulations were  
595 conducted with modified plant C:P stoichiometry (Plant C:P: *SENS1*), P uptake scaling factor (K<sub>P</sub>) (K<sub>P</sub>: *SENS2*),  
596 inorganic (K<sub>P\_sorb\_in</sub>: *SENS3*) and organic (K<sub>P\_sorb\_or</sub>: *SENS4*) P adsorption coefficients  
597 (K<sub>sorb-or</sub>, K<sub>sorb-in</sub>), and maximum inorganic (K<sub>P\_sorb\_in\_max</sub>: *SENS5*) and organic (K<sub>P\_sorb\_or\_max</sub>:  
598 *SENS6*) sorbed P (K<sub>or-max</sub>, K<sub>in-max</sub>). These values were prescribed to vary between ±50% of the observed  
599 values and their effect on C pools (plant and soil C) and fluxes (NPP and excess C), and P pools (plant, soil, and  
600 soil sorbed P) was assessed. As the derived model parameters from measurements have their own level of  
601 uncertainty, we took the 50% of the change to test these parameters at reasonable degree. However, the  
602 occluded and weathered P pools are prescribed for this model application, the occluded and weather P  
603 coefficients (other two P-related model parameters) were not part of sensitivity tests.

604

605 Our model evaluation period is limited to years 2017-18 due to the P measurement availability. However, in  
606 order to perform inter-models comparison with 15 models studied by Fleischer *et al.*, (2019) we also studied the  
607 response of GPP, NPP and BP to eCO<sub>2</sub> for both initial (1999) and 15 years periods (between 1999-2013).

608

609

### 610 3. Results

611

#### 612 3.1 Model application under ambient CO<sub>2</sub>

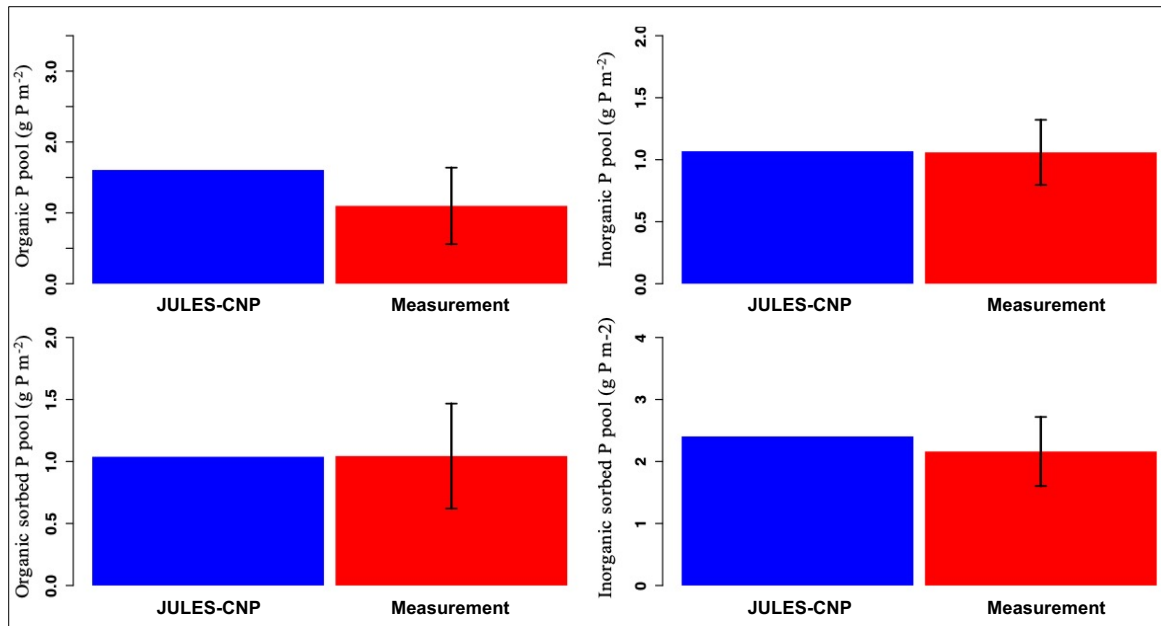
613

##### 614 3.1.1 Calibration of simulated soil P pools

615

616 The maximum sorption capacities ( $P_{in-max_n}$ ,  $P_{or-max_n}$ , eq.37 and 40) were calibrated to the observed P pools.  
617 As a result, JULES-CNP could reproduce the measured soil p pools (Figure. 2 and Table 4). Simulated  
618 inorganic soil P and sorbed organic and inorganic soil P closely matched the observations (Table 5 and Figure.  
619 2). However, simulated organic soil P overestimates the observations by 60 %.

620



621  
622 **Figure 2-** Modelled vs measured soil phosphorus pools under ambient CO<sub>2</sub> (for the soil depth of 0-30cm). Black line  
623 represents standard deviation  
624

625  
626 **Table 4.** Observed and simulated phosphorus pools and fluxes. Occluded and weathered P pools were prescribed using the  
627 observed values (between period 2017-18).

	Phosphorus pools and fluxes		
	Measured	Modelled Ambient CO <sub>2</sub>	Modelled Elevated CO <sub>2</sub>
<b>Organic P</b> (g P m <sup>-2</sup> )	1.09±0.53	1.6	1.57
<b>Inorganic P</b> (g P m <sup>-2</sup> )	1.05±0.33	1.07	0.96
<b>Sorbed organic P</b> (g P m <sup>-2</sup> )	1.04±0.42	1.04	1.03
<b>Sorbed inorganic P</b> (g P m <sup>-2</sup> )	2.1±0.55	2.4	2.4
<b>Occluded P</b> (g P m <sup>-2</sup> )	7.98±2.38	prescribed	prescribed
<b>Weathered P</b> (g P m <sup>-2</sup> )	0.59±12	prescribed	prescribed
<b>Total vegetation P</b> (g P m <sup>-2</sup> )	4.15	4.66	5.11
<b>Soil P – 30cm</b> (g P m <sup>-2</sup> )	13.85	14.7	14.56
<b>Total ecosystem P</b> (g P m <sup>-2</sup> )	-	35.97	35.97
<b>P litter flux</b> (g P m <sup>-2</sup> yr <sup>-1</sup> )	0.3	0.28	0.29

628  
629  
630 **3.1.2 Model evaluation**

631  
632 JULES CNP-CNP could reproduce the plant and soil C (Figure.2 and Table 5) and N pools and fluxes (Figure  
633 S6 and Table 6) pools and fluxes under ambient CO<sub>2</sub>. Our results show that simulated GPP, is within the range  
634 of measurement (3.02 kg C m<sup>-2</sup> yr<sup>-1</sup> model vs 3-3.5 kg C m<sup>-2</sup> yr<sup>-1</sup> observed, respectively, Table 5).  
635

636 Simulated NPP, is close to the measured values (NPP: 1.14 - 1.31 observed vs 1.26 modelled kg C m<sup>-2</sup> yr<sup>-1</sup>) with  
637 autotrophic respiration (RESP) also closely following the observations (1.98 observed vs 1.81 modelled kg C m<sup>-2</sup>  
638 yr<sup>-1</sup>). Biomass production is estimated as a difference between NPP and the amount of C which is not fixed by  
639 plants due to the insufficient P in the system (excess C) (eq. 27). The excess C flux is highly dependent on the  
640 plant P and the overall P availability to satisfy demand (Table 5). Simulated flux of excess C is 0.3 kg C m<sup>-2</sup> yr<sup>-1</sup>  
641 under ambient CO<sub>2</sub>. In JULES-CNP this flux is subtracted from NPP in order to give the BP (eq. 17) (Table 5).  
642 Our simulated litterfall overestimates the observations by 32%, however simulated vegetation and its  
643 components (fine root, leaf and wood) and soil C stocks match well the observations (Table 5).

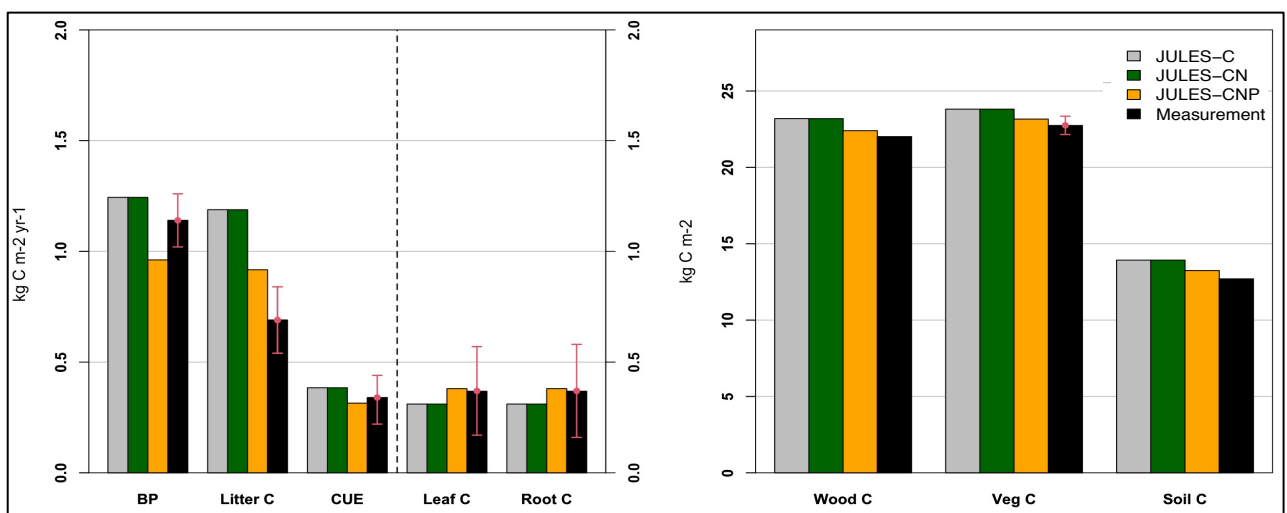


644 **Table 5.** Observed and simulated carbon pools and fluxes with JULES\_CNP (between period 2017-18)

<b>Carbon pools and fluxes</b>			
	<b>Measured</b>	<b>Modelled Ambient CO<sub>2</sub></b>	<b>Modelled Elevated CO<sub>2</sub></b>
<b>GPP</b> (kg C m <sup>-2</sup> yr <sup>-1</sup> )	3.0 – 3.5	3.06	3.9
<b>NPP<sub>pot</sub></b> (kg C m <sup>-2</sup> yr <sup>-1</sup> )	-	1.27	1.77
<b>Plant respiration</b> (kg C m <sup>-2</sup> yr <sup>-1</sup> )	1.98	1.78	2.12
<b>Excess C flux</b> (kg C m <sup>-2</sup> yr <sup>-1</sup> )	-	0.30	0.81
<b>Biomass Production</b> (kg C m <sup>-2</sup> yr <sup>-1</sup> )	1.14±0.12	0.96	0.94
<b>Litter C flux</b> (kg C m <sup>-2</sup> yr <sup>-1</sup> )	0.69±0.15	0.91	0.83
<b>Leaf C</b> (kg C m <sup>-2</sup> )	0.37±0.2	0.38	0.40
<b>Wood C</b> (kg C m <sup>-2</sup> )	22.01	22.4	24.71
<b>Root C</b> (kg C m <sup>-2</sup> )	0.37±0.2	0.38	0.40
<b>Vegetation C</b> (kg C m <sup>-2</sup> )	22.75±0.3	23.16	25.52
<b>Soil C stock</b> (kg C m <sup>-2</sup> )	12.7	13.2	12.71
<b>LAI</b> (m <sup>2</sup> m <sup>-2</sup> )	5.6±0.36	5.77	6.12

645  
646 **3.1.3 Comparison of JULES C, CN and CNP under ambient CO<sub>2</sub>**  
647

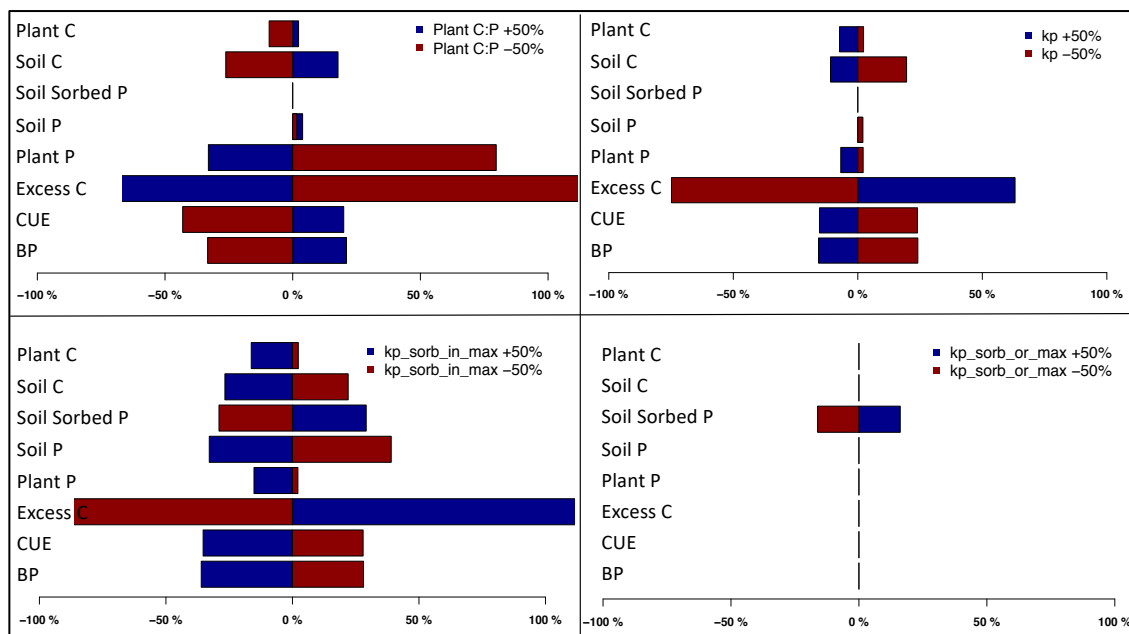
648 We compare simulated C pools and fluxes from JULES-C, JULES-CN and JULES-CNP (Figure. 3). There is no  
649 difference between C stocks and fluxes in simulations from JULES C and CN indicating that there is no N  
650 limitation at this tropical site in the CN simulations. However, simulated BP and litter flux of C by JULES  
651 C/CN are higher than in JULES-CNP but also overestimate the observations (litter flux of JULES C/CN: 1.18,  
652 JULES CNP: 0.91 and obs 0.69 (kg C m<sup>-2</sup> yr<sup>-1</sup>) and BP of JULES C/CN: 1.24, JULES CNP: 0.96 and obs 1.14-  
653 1.31 (kg C m<sup>-2</sup> yr<sup>-1</sup>), respectively). By including the P cycling in JULES an excess C flux of 0.3 (kg C m<sup>-2</sup> yr<sup>-1</sup>)  
654 is simulated, indicating a 24% P limitation to BP at this site according to JULES CNP, which represents a 29%  
655 decrease in BP compared to JULES-C/CN. Consequently, the total vegetation C stock for models without P  
656 inclusion is higher than the CNP version (+3% difference) due to the lack of representation of P limitation. The  
657 simulated soil C stock in JULES C and JULES CN is also higher than in the CNP version (JULES C/CN: 13.93  
658 vs. JULES CNP: 13.18 (kg C m<sup>-2</sup> yr<sup>-1</sup>)) and higher than the observations. Moreover, CUE in JULES C/CN  
659 (eq.54) is higher than observations and JULES CNP version (JULES C/CN: 0.38 vs. JULES CNP: 0.31, obs:  
660 0.34 ±0.1(dimensionless)).  
661  
662



663  
664 **Figure. 3-** JULES C, CN, CNP modelled vs measured C pools (Leaf, root, wood, Veg and Soil C) (in kg C m<sup>-2</sup>)  
665 and fluxes (BP and Litter C) (in kg C m<sup>-2</sup> yr<sup>-1</sup>) and CUE under ambient CO<sub>2</sub>. Note that CUE is unitless.  
666  
667  
668

669 **3.1.4 Model sensitivity**

670  
 671 The results indicate that among all the corresponding C and P pools and fluxes, the excess C flux – which  
 672 demonstrates P limitation to growth – shows the highest sensitivity to changes in C:P ratios,  $K_P$  and  
 673  $K_{or-max}$ ,  $K_{in-max}$ . A decrease in plant C:P results in a large increase in excess C. This is due to the higher plant  
 674 P demand as a result of lower plant C:P ratios. An increase in the uptake factor and maximum sorbed organic  
 675 and inorganic P also results in an increase in excess C. This is due to the higher uptake demand through higher  
 676 uptake capacity (due to higher  $K_P$ ) and lower available P for uptake due to higher organic and inorganic sorbed  
 677 P (due to higher  $K_{or-max}$ ,  $K_{in-max}$ ). Since the total P in the system is lower than the plant demand, the uptake  
 678 capacity and sorbed P, higher P limitation is placed on growth (decreasing BP) which results in an increase in  
 679 excess C and decrease in plant C, but also soil C which is a result of lower litter input (Figure 4). Total soil P  
 680 shows low sensitivity to changes in plant C:P and uptake factor but high sensitivity to maximum inorganic  
 681 sorbed P. Moreover, sorbed P shows middle to high sensitivity to maximum organic and inorganic sorbed P  
 682 respectively (Figure. S5). Nevertheless, organic and inorganic P adsorption coefficients ( $K_{sorp-or}$ ,  $K_{sorp-in}$ )  
 683 show no sensitivity to C and P pools and fluxes. This is due to limiting the organic and inorganic P sorption  
 684 terms controlled only by maximum sorption, hence no effect applied by organic and inorganic adsorption  
 685 coefficients.  
 686



687  
 688 **Figure. 4-** Model sensitivity test results and corresponding C and P pools and fluxes under ambient CO<sub>2</sub>.  
 689

690  
 691 **3.2 Model application under elevated CO<sub>2</sub>**  
 692

693 **3.2.1 Simulated plant and soil C and P pools and fluxes -JULES CNP: eCO<sub>2</sub> vs ambient CO<sub>2</sub>**  
 694

695 The eCO<sub>2</sub> simulation using JULES CNP yields a higher GPP compared to the ambient CO<sub>2</sub> (0.83 (kg C m<sup>-2</sup> yr<sup>-1</sup>)  
 696 increase), as a result of CO<sub>2</sub> fertilization. Moreover, due to the GPP increase, NPP and RESP follows the same  
 697 trend and increased compared to ambient CO<sub>2</sub> (NPP: 0.49 and RESP:0.3 (kg C m<sup>-2</sup> yr<sup>-1</sup>) increase) (Table 5). The  
 698 total simulated vegetation C pool increases under eCO<sub>2</sub> compared to ambient CO<sub>2</sub> (0.41 kg C m<sup>-2</sup>), hence the  
 699 estimated plant P (estimated as a fraction of C:P ratios) increases as well (+0.45 (g P m<sup>-2</sup>)) (Fig 6, Table 4).  
 700 Thus, the simulated plant P demand is higher, and as the total available soil P for uptake is limited, the simulated  
 701 excess C flux increases to 0.51(kg C m<sup>-2</sup> yr<sup>-1</sup>). Moreover, despite the higher NPP under eCO<sub>2</sub> compared to  
 702 simulated NPP under ambient CO<sub>2</sub>, due to the substantial increase in simulated excess C, the BP is similar to the  
 703 ambient CO<sub>2</sub> (2% difference).  
 704  
 705  
 706  
 707

708 The simulated organic soil P under eCO<sub>2</sub> yields close to the ambient CO<sub>2</sub> (1.6 g P m<sup>-2</sup>) (Table 5). This is due to  
 709 the same parameterization of the output fluxes from this pool for eCO<sub>2</sub> and ambient CO<sub>2</sub>. The simulated pool of  
 710 inorganic P under eCO<sub>2</sub> decreases compared to the ambient CO<sub>2</sub> by 0.11 (g P m<sup>-2</sup>) due to the increased plant P  
 711 pools and slight increase in uptake (+0.13 %).  
 712 However, the simulated sorbed organic and inorganic soil P from eCO<sub>2</sub> are similar to those simulated under the  
 713 ambient CO<sub>2</sub> which is due to the same parameterizing of sorption function (maximum sorption capacity) from  
 714 the ambient CO<sub>2</sub> run as explained in calibration section. Moreover, the modelled occluded and weathered soil P  
 715 yield similar to those in the ambient CO<sub>2</sub> simulation (Table 5) which is due to the same prescribed observational  
 716 data that was used for this simulation.

### 717 3.2.2 Comparison of JULES C, CN and CNP under elevated CO<sub>2</sub>

718 JULES C/CN show higher vegetation and soil C pools, BP and litter flux compared to JULES-CNP: (Table 6,  
 719 Figure. S2). Under eCO<sub>2</sub>, simulated NPP using JULES C-CN is 4.5% higher than JULES CNP and the BP with  
 720 JULES- C/CN is 96.8% higher than in JULES-CNP which simulates an excess C flux of 0.81 (kg C m<sup>-2</sup> yr<sup>-1</sup>)  
 721 equivalent to 46% P limitation under eCO<sub>2</sub>. As a result of P limitation and eCO<sub>2</sub>, the simulated CO<sub>2</sub> fertilization  
 722 effect estimated based on changes in biomass under ambient and eCO<sub>2</sub> was reduced from 13% with JULES-  
 723 C/CN to 10% JULES-CNP. Moreover, the CUE from JULES C/CN is 87.5% higher than the JULES CNP as a  
 724 result of high P limitation over biomass production.  
 725  
 726

727 **Table 6.** C pools and fluxes using JULES C/CN and difference in percentage with JULES CNP model under eCO<sub>2</sub>. A  
 728 positive % means larger respective values simulated with JULES C and JULES CN than with JULES CNP (between period  
 729 2017-18).  
 730

	GPP	NPP	BP	CUE	Litter C	Leaf C	Root C	Wood C	Soil C
JULES C/CN	4.1	1.85	1.85	45%	1.77	0.42	0.42	26.1	19.2
JULES CNP	3.9	1.77	0.94	24%	0.83	0.4	0.4	24.71	12.71
ΔC/CN: CNP	5.1%	4.5%	96.8%	87.5%	113.3%	5%	5%	5%	51.1%

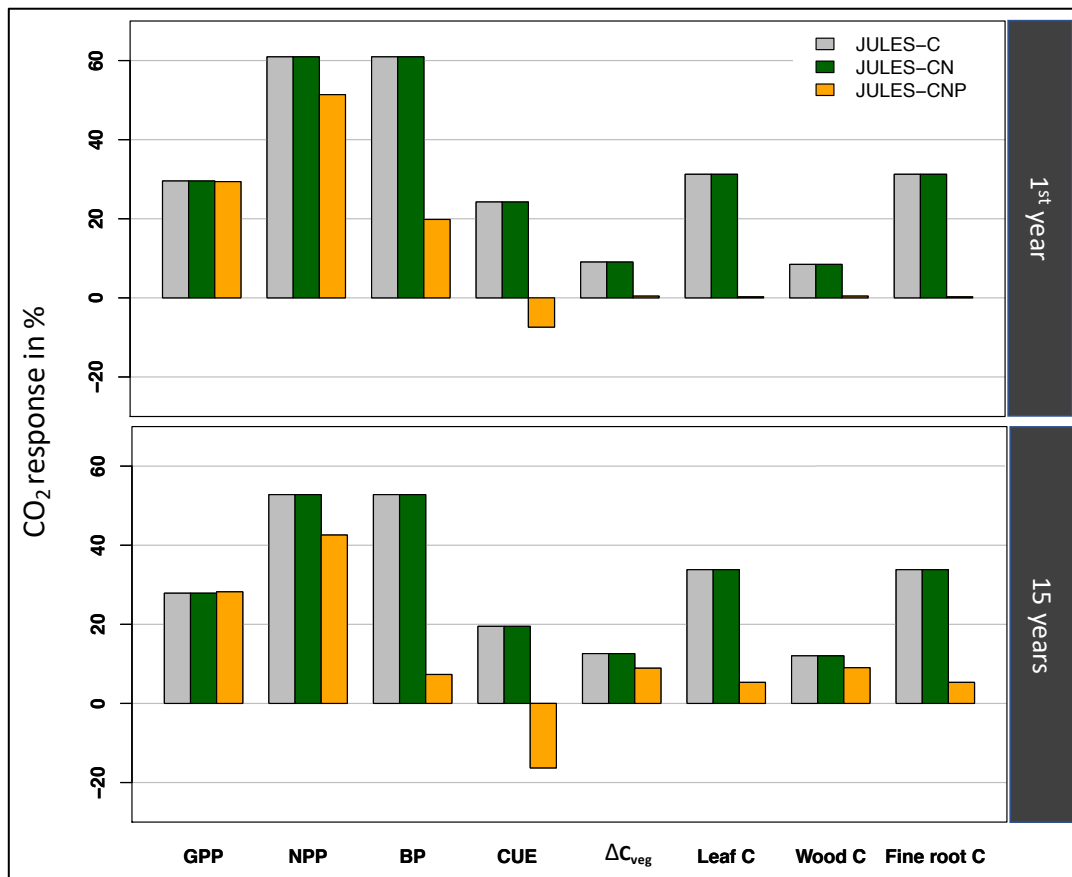
#### 731 3.2.2.1 Inter-models under elevated CO<sub>2</sub>

732 Following Fleischer *et al.*, (2019), we report the simulated response to eCO<sub>2</sub> for year 1999 (initial: CO<sub>2</sub> effect)  
 733 and 1999-2013 (15 years: final effect) which are different than our evaluation period (2017-18). Using JULES C  
 734 and JULES CN under eCO<sub>2</sub>, simulated GPP and NPP during the 1<sup>st</sup> year increase by 30% and 61% respectively  
 735 and by 28% and 52% after 15 years (Figure. 5). However, using JULES CNP, eCO<sub>2</sub> increases simulated GPP,  
 736 NPP and BP responses during the 1<sup>st</sup> year by 29%,51% and 20% and by 28%, 43% and 7%, after 15 years  
 737 respectively.  
 738

739 Corresponding simulated CUE during the 1<sup>st</sup> year and 15 years shows an increase of 24% and 20% in response  
 740 to eCO<sub>2</sub> using JULES C/CN respectively. However, using JULES CNP, simulated CUE for the 1<sup>st</sup> and after 15  
 741 years is reduced by 7% and 17% in response to eCO<sub>2</sub>.  
 742

743 Simulated total biomass (leaf, fine root and wood C) (ΔC<sub>veg</sub>) using JULES C/CN for the 1<sup>st</sup> and 15 years of  
 744 eCO<sub>2</sub> increases by 9% and 13% respectively. However, using JULES CNP ΔC<sub>veg</sub> only increases by 0.5% and  
 745 9% for 1<sup>st</sup> and 15 years of eCO<sub>2</sub>, respectively.  
 746  
 747

748  
 749



750 **Figure. 5-** Relative effect of eCO<sub>2</sub> on simulated GPP, NPP, BP, CUE, ΔC<sub>veg</sub>, leaf C and fine root C, using three  
751 versions of JULES model in 1<sup>st</sup> (initial response) and 15 years periods (final response).  
752  
753

### 754 3.3 Plant P Demand, uptake and excess C under ambient and elevated CO<sub>2</sub>

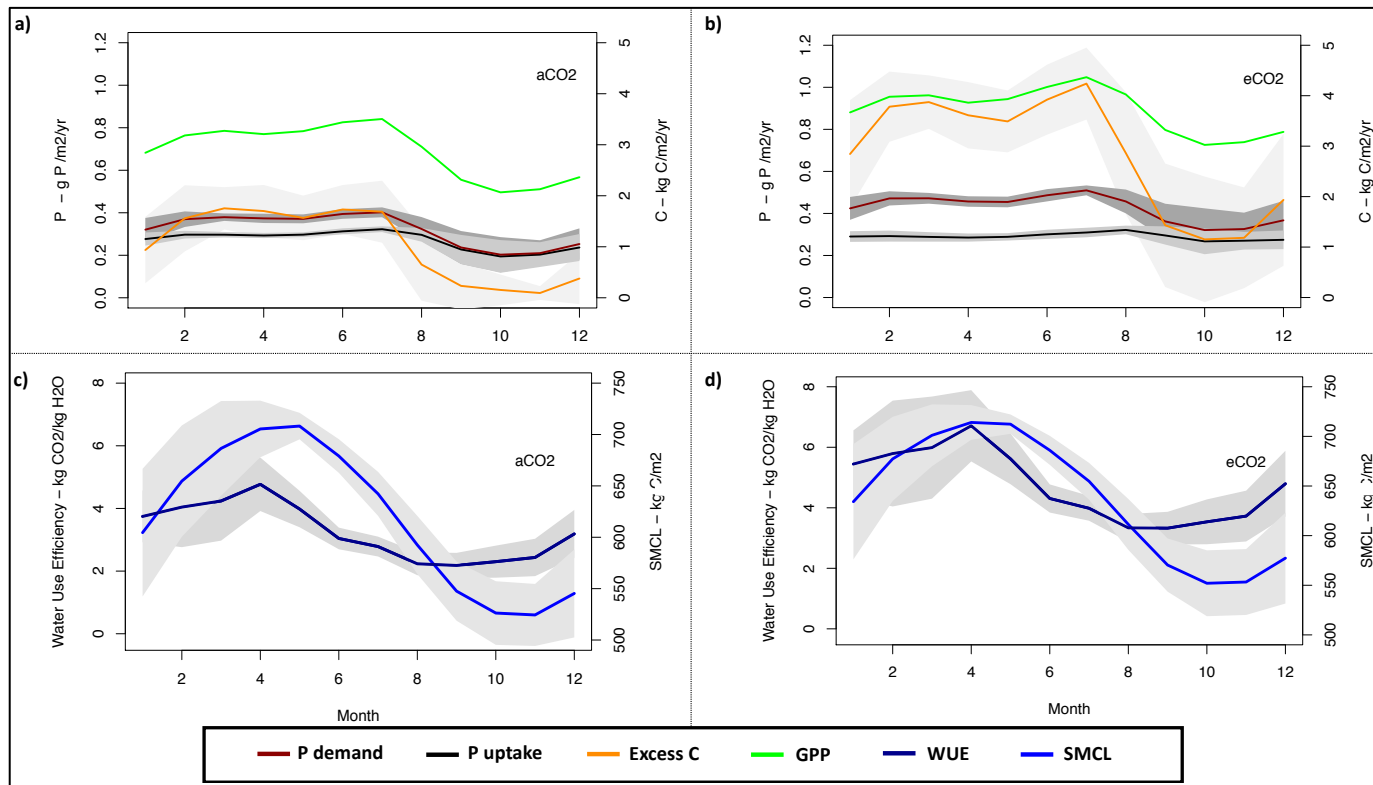
755 To understand further the CP-cycle dynamics, we studied the monthly averaged plant P demand and the relative  
756 (limited) P uptake (eq. 26) under both ambient and elevated CO<sub>2</sub> conditions (Figure. 6).  
757  
758  
759

760 Under ambient CO<sub>2</sub> condition the highest GPP is estimated at  $3.5 \pm 0.19$  kg C m<sup>-2</sup> month<sup>-1</sup> in July and the lowest  
761 at  $2.06 \pm 0.61$  kg C m<sup>-2</sup> month<sup>-1</sup> in October (Figure. 6-a). The estimated WUE and SMCL in October is among the  
762 lowest estimated monthly values at  $2.3 \pm 0.51$  kg CO<sub>2</sub>/kg H<sub>2</sub>O and  $526.2 \pm 31$  kg m<sup>-2</sup> respectively (Figure. 6-c).  
763 The highest P demand is estimated at  $0.4 \pm 0.02$  g P m<sup>-2</sup> month<sup>-1</sup> in July and the lowest demand at  $0.2 \pm 0.08$  g P m<sup>-2</sup>  
764 month<sup>-1</sup> in October. Consequently, the highest and lowest uptake ( $0.32 \pm 0.01$  and  $0.19 \pm 0.07$  g P m<sup>-2</sup> month<sup>-1</sup>,  
765 respectively). The excess C for the highest and lowest GPP and demand periods are estimated at  $0.4 \pm 15$  and  
766  $0.04 \pm 0.07$  kg C m<sup>-2</sup> month<sup>-1</sup>, respectively.  
767

768 However, similar to ambient CO<sub>2</sub>, under eCO<sub>2</sub> condition the highest estimated GPP is in July at  $4.36 \pm 0.21$  kg C  
769 m<sup>-2</sup> month<sup>-1</sup> and lowest for October  $3.02 \pm 0.75$  kg C m<sup>-2</sup> month<sup>-1</sup> (Figure. 6-b). The estimated WUE and soil  
770 moisture content (SMCL) for the lowest GPP period is among the lowest monthly estimated values at  $3.5 \pm 0.74$   
771 kg CO<sub>2</sub>/kg H<sub>2</sub>O and  $552 \pm 33$  kg m<sup>-2</sup> for October respectively (Figure. 6-d). The highest P demand is estimated  
772 for July at  $0.51 \pm 0.02$  g P m<sup>-2</sup> month<sup>-1</sup> with the uptake flux of  $0.31 \pm 0.02$  g P m<sup>-2</sup> month<sup>-1</sup> and the lowest demand  
773 is estimated for October at  $0.32 \pm 0.1$  g P m<sup>-2</sup> month<sup>-1</sup> with the estimated uptake flux of  $0.26 \pm 0.06$  g P m<sup>-2</sup> month<sup>-1</sup>.  
774 The highest excess C flux is also for July at  $1.01 \pm 0.17$  kg C m<sup>-2</sup> month<sup>-1</sup> and lowest for October  $0.27 \pm 0.29$  kg  
775 C m<sup>-2</sup> month<sup>-1</sup>, respectively.  
776

777 However, despite the P limitation in both eCO<sub>2</sub> and ambient CO<sub>2</sub> conditions, the P uptake flux under eCO<sub>2</sub> is  
778 higher than the ambient CO<sub>2</sub> condition. This is due to the higher WUE and increased SMCL (controlling uptake  
779 capacity (eq. 27)) under eCO<sub>2</sub> condition, hence more water availability during the dry season to maintain  
780 productivity and critically transport P to the plant (see eq. 27), compared to ambient CO<sub>2</sub> condition (Figure. 6-c  
781 and d). Additionally, in JULES both the vertical discretisation (Burke, Chadburn and Ekici, 2017) and

782 mineralisation terms (Wiltshire *et al.*, 2021) depend on the soil moisture and temperature. Thus, higher P  
 783 concentration and uptake under eCO<sub>2</sub> condition.  
 784



785  
 786 **Figure. 6-** Simulated monthly plant P demand and uptake ( $\text{g P m}^{-2} \text{ yr}^{-1}$ ), excess C and GPP ( $\text{kg C m}^{-2} \text{ yr}^{-1}$ ) under a) aCO<sub>2</sub>  
 787 and b) eCO<sub>2</sub>, water use efficiency ( $\text{g m}^{-2} \text{ yr}^{-1}$ ) under c) ambient CO<sub>2</sub> (aCO<sub>2</sub>) and d) eCO<sub>2</sub> conditions. The grey area represents  
 788 the standard deviation.  
 789

### 790 3.4 Soil P pools profile under ambient CO<sub>2</sub> and elevated CO<sub>2</sub>

791 We explored the distribution of the inorganic and organic soil P and their sorbed fraction within the soil layers  
 792 and under different CO<sub>2</sub> conditions (Figure. S3). Both the ambient and eCO<sub>2</sub> simulations have a close inorganic  
 793 soil P distribution at the topsoil layer (0-30cm) (0.85 vs. 0.9 ( $\text{g P m}^{-2}$ ) respectively) as well as similar organic  
 794 soil P distribution (0.85 vs 0.9 ( $\text{g P m}^{-2}$ ) respectively).  
 795

796 However, the organic soil P and sorbed forms of inorganic and organic soil P profiles are not changing  
 797 significantly between different sets due to the similar parameterization of the processes that control these pools  
 798 (processes which are related to the physical aspects of soils, hence not changing under eCO<sub>2</sub> condition) and the  
 799 same parameter values used for both ambient and eCO<sub>2</sub> runs.  
 800

801 Moreover, the soil P within 30cm soil depth for ambient and eCO<sub>2</sub> conditions is at 14.7 ( $\text{g P m}^{-2}$ ) and 14.56 ( $\text{g P}$   
 802  $\text{m}^{-2}$ ) respectively, and the total ecosystem P for both ambient and eCO<sub>2</sub> conditions is at 35.97 ( $\text{g P m}^{-2}$ ).  
 803 However, the slightly lower soil P in the eCO<sub>2</sub> condition is due to the higher plant P demand compared to the  
 804 ambient condition, hence the higher allocated P vegetation (10%) under eCO<sub>2</sub> condition.  
 805

## 806 4. Discussion

807  
 808 Studies show the significant role of the tropical forests, and Amazonia in particular, in C uptake and regulating  
 809 atmospheric CO<sub>2</sub> (Brienen *et al.*, 2015; Phillips *et al.*, 2017). As soil P availability is low in the majority of  
 810 Amazonia (Quesada *et al.*, 2012), the competition for nutrients by both plant and soil communities is high  
 811 (Lloyd *et al.*, 2001). The responses of these communities to eCO<sub>2</sub> under P limited conditions remains uncertain  
 812 (Fleischer *et al.*, 2019). These responses in P enabled models are represented in different ways regarding the  
 813 excess C which is not used for plant growth due to P limitation. Either growth is directly downregulated taking  
 814 the minimum labile plant C,N and P (Goll *et al.*, 2017), or photosynthesis is downregulated via  $V_{\text{cmax}}$  and  $J_{\text{max}}$   
 815 (Comins and McMurtrie, 1993; Yang *et al.*, 2014; Zhu *et al.*, 2016) and finally models like JULES CNP  
 816  
 817

818 downregulate NPP via respiration of excess carbon that cannot be used for growth due to plant nutrient  
819 constraints (Haverd *et al.*, 2018). The estimated CUE depends on the modelling approach. Models that down  
820 regulate the photosynthetic capacity and GPP consequently (Comins and McMurtrie, 1993; Yang *et al.*, 2014;  
821 Zhu *et al.*, 2016), simulate a positive CUE response to CO<sub>2</sub> fertilization while models that down regulate the  
822 NPP and respire the excess C (Haverd *et al.*, 2018) simulate a negative CUE response (Fleischer *et al.*, 2019)  
823 which is in line with the studies showing lower CUE when nutrient availability declines (Vicca *et al.*, 2012).  
824 However, this remains a major uncertainty in understanding the implication of P limitation on terrestrial  
825 biogeochemical cycles.

826 Our new developments include major P processes in both plant and soil pools and can be applied to the Amazon  
827 region using existing soil (Quesada *et al.*, 2011) and foliar structural and nutrient (Fyllas *et al.*, 2009) data for  
828 parameterisation. Moreover, JULES CNP can be applied at the global scale and for future projections using  
829 global soil P data (Sun *et al.*, 2021) for model initialization and PFT-specific plant stoichiometries  
830 (Zechmeister-Boltenstern *et al.* 2015), soil stoichiometries (Zechmeister-Boltenstern *et al.* 2015; Tipping *et al.*  
831 (2016), sorption and weathering ratios (based on lithological class specific from the Glim lithological map  
832 (Hartmann and Moosdorf, 2012) and soil shielding from Hartmann *et al.*, (2014)).

833

834 **4.1. Evaluation of model performance against observations**

835

836 JULES-CNP could reproduce the magnitude of soil organic and inorganic P pools and fluxes. The relative  
837 distribution of total organic P, total inorganic P and residue P fractions of total P in soils under Brazilian  
838 Eucalyptus plantations (Costa *et al.*, 2016) shows inorganic P fraction of 28% from total soil P which is close to  
839 our estimation of 24% and organic P fraction of 30% from total soil P which is higher than our estimated  
840 fraction of 18%. Thus, we may need to improve the process representation or parameters that control the organic  
841 P concentration, such as litter flux and decomposition, soil organic P mineralization, and immobilization in the  
842 future.

843

844 Our estimated maximum P uptake, which represents the actual available P for plant uptake (Goll *et al.*, 2017),  
845 for both ambient and eCO<sub>2</sub> conditions, is highly correlated with the plant P demand ( $R^2 = 0.96$  and  $0.52$   
846 respectively). The plant P demand depends on the GPP changes which are reflected by the WUE (Hatfield and  
847 Dold, 2019). Hence, under ambient CO<sub>2</sub>, JULES CNP simulates lower GPP and plant P demand during the dry  
848 season than during the wet season. Sufficient P uptake during these periods results in the lowest P limitation,  
849 thus the lowest simulated excess C. Nevertheless, under eCO<sub>2</sub> the same pattern is simulated but a higher  
850 availability of soil P due to the stomatal closure in the dry season. Hence, due to the plant's more efficient water  
851 usage, the soil moisture in the dry season is higher (Xu *et al.*, 2016) which impacts our capped P uptake flux (eq.  
852 27) and increases the uptake capacity respectively.

853

854 Overall, JULES-CNP reproduced the observed C pools and fluxes which are in the acceptable ranges compared  
855 to the measurements. However, using the JULES default  $V_{\text{cmax}}$  estimation method (eq. 40), the model slightly  
856 underestimates the total GPP ( $2.9 \text{ kg C m}^{-2} \text{ yr}^{-1}$  vs.  $3\text{-}3.5 \text{ kg C m}^{-2} \text{ yr}^{-1}$ ). Therefore, in this version of the model,  
857 we used the improved  $V_{\text{cmax}}$  estimation method based on N and P (eq. 46) which resulted a final estimated GPP  
858 closer to the measurements ( $3.06 \text{ kg C m}^{-2} \text{ yr}^{-1}$ ).

859

860 Our results show an increase in GPP (21%) in response to eCO<sub>2</sub> which is higher than the average increase of  
861 GPP reported in mature eucalyptus forests (11%), also growing under low P soils at the free air CO<sub>2</sub> enrichment  
862 experiment (EucFACE) facility in Australia (Jiang *et al.*, 2020). This can be related to the lower decrease of  
863 biomass growth response estimated by JULES-CNP (-3%) compared to the measurements from mature forests  
864 (-8%) (Ellsworth *et al.*, 2017), due to the P limitation which showed to impact the above-ground biomass  
865 growth response in mature forests (Körner *et al.*, 2005; Ryan, 2013; Klein *et al.*, 2016).

866

867 In order to estimate the biomass production (BP), we deducted the excess C fluxes from the NPP. Using JULES  
868 C/CN models our estimated biomass productivity enhancement due to eCO<sub>2</sub> (49%) is in the middle range of the  
869 reported various studies from different biomes by Walker *et al.*, (2021). Moreover, our estimated difference of  
870 BP between ambient and eCO<sub>2</sub> conditions (2%) is close to the estimated difference for mature forests (3%)  
871 (Jiang *et al.*, 2020).

872 A global estimation for tropical forests using CASACNP model which includes N and P limitations on  
873 terrestrial C cycling, shows that NPP is reduced by 20% on average due to the insufficient P availability (Wang,  
874 Law and Pak, 2010) which is close to our estimated P limitation of 24%. This finding is in line with  
875 experimental study that shows a strong correlation between the total NPP and the soil available P (Aragão *et al.*,  
876 2009). Nevertheless, our model show that the P limitation mimics the same response to the CO<sub>2</sub> fertilization  
877 similar to sites in pool soils (see ZAR-01 site in Aragão *et al.*, (2009)). The estimated decrease of NPP in

878 response to eCO<sub>2</sub> as a result of P limitation is in line with the findings from CLM-CNP model at five tropical  
879 forests (Yang *et al.*, 2014) which indicates the CO<sub>2</sub> fertilization dependency on the processes that affect P  
880 availability or uptake.

881  
882 Our estimated CUE (0.31) is close to the estimation by Jiang *et al.* (2020) for mature forests (0.31±0.03), as well  
883 as to the measurement for our study site (0.34 ±0.1). There is currently a lack of representation of stand age in  
884 JULES-CNP which can significantly change this ratio (e.g. mature trees are less responsive to the nutrient  
885 limitations) (De Lucia *et al.*, 2007; Norby *et al.*, 2016). However, a recent development of Robust Ecosystem  
886 Demography (RED) model into JULES (Argles *et al.*, 2020) and its integration into JULES-CNP in the future  
887 can resolve this issue. Moreover under low P availability, all available P is considered to be adsorbed or taken  
888 by plant and microbes for further consumption, with leaching considered to be minor within the time scales of  
889 our study period (Went and Stark, 1968; Bruijnzeel, 1991; Neff, Hobbie and Vitousek, 2000).

890 Due to the strong fixation of P in the soil (Aerts & Chapin, 2000; Goodale, Lajtha, Nadelhoffer, Boyer, &  
891 Jaworski, 2002), the P deposited is unlikely to be available to plants in the short term (de Vries *et al.*, 2014), for  
892 this reason this version of JULES CNP did not include P deposition. However both P deposition and leaching  
893 are likely to have a very important role on sustaining the productivity of tropical forests in the Amazon over  
894 longer time scales (Van Langenhove *et al.*, 2020) and needs to be considered in future studies.

895 Moreover, biochemical mineralisation is not included in the current version of JULES CNP and it only accounts  
896 for total mineralization. However, even the models which includes this process, show no significant difference  
897 between total and biochemical mineralized P which can be due to complexity of identifying the inclination of  
898 mineralization versus uptake (Martins *et al.*, 2021).

899 Lastly, in order to capture plant internal nutrient impact on the C storage, the future work should focus on  
900 implanting a recent developed Non-Structural Carbohydrate (NSC) model (SUGAR) (Jones *et al.*, 2020) in  
901 JULES-CNP.

902

#### 903 **4.2. Inter-models comparison**

904

905 The comparison of simulated GPP enhancement across JULES versions for the 1<sup>st</sup> year is within the middle  
906 range of the 1<sup>st</sup> year CO<sub>2</sub> responses of the C/CN models studied by Fleischer *et al.*, (2019) evaluating simulated  
907 eCO<sub>2</sub> effects at a site in Manaus using the same meteorological forcing and methodology used in this study for  
908 a range of DGVM's. However, comparison for 15 years of eCO<sub>2</sub>, shows that the simulated response with  
909 JULES CNP is on the higher end of Fleischer *et al.*, (2019) study which is due to the higher estimated biomass  
910 growth by JULES CNP (Table S1). Similarly, using JULES CNP our estimated GPP enhancement is on the  
911 higher end of model estimations in Fleischer *et al.*, (2019). Moreover, comparing the GPP responses between  
912 different versions of (JULES C/CN and CNP), the JULES CNP shows a slightly higher response to CO<sub>2</sub>  
913 fertilization associated with the higher WUE changes (Xiao *et al.*, 2013) (Figure. S4). This is due to the higher  
914 sensitivity of the plant to water availability than the P availability in the P limited system (He and Dijkstra,  
915 2014). Hence, under eCO<sub>2</sub> due to water-saving strategy of plants and stomatal closure (Medlyn *et al.*, 2016),  
916 simulated transpiration is decreased (Sampaio *et al.*, 2021) and photosynthesis is enhanced compared ambient  
917 CO<sub>2</sub>.

918

919 To that end, the monthly changes of WUE in JULES CNP are highly correlated to the GPP, hence the lowest  
920 and highest WUE follow the same periods as GPP similar to responses captured with models studied by  
921 Fleischer *et al.*, (2019) (Table. S1).

922

923 Our estimated NPP enhancement using JULES C/CN models for both 1<sup>st</sup> and 15 years period is within the  
924 middle range of the models in Fleischer *et al.*, (2019). Nevertheless, JULES CNP response of BP is in the lower  
925 band of the CNP models by Fleischer *et al.*, (2019) and close to the estimations from CABLE (Haverd *et al.*,  
926 2018) and ORCHIDEE (Goll *et al.*, 2017) models, which may be due to the similar representation of P processes  
927 and limitation between these models. However, our results show a 29% decrease in NPP using JULES-CNP  
928 compared to JULES-C/CN which is smaller than the differences between the CLM-CNP and CLM-CN versions  
929 (51% decrease) (Yang *et al.*, 2014). The lower estimated decrease in JULES highlights the need to further study  
930 the fully corresponding plant C pools and fluxes to the changes in soil and plant P. Therefore, future work  
931 should be focused on the improvement of the total P availability and the plant C feedbacks. Moreover, there are  
932 other environmental factors such as temperature which shows a possible impact on the CO<sub>2</sub> elevation and the  
933 changes of NPP (Baig *et al.*, 2015) which needs further improvement in our model.

934 The CUE estimations of 1<sup>st</sup> year and 15 years response to CO<sub>2</sub> elevation from JULES C/CN are in the middle  
935 range of C/CN models in Fleischer *et al.*, (2019). However, the estimated CUE using JULES CNP for 1<sup>st</sup> and 15  
936 years are in the low range of CNP models reported by Fleischer *et al.*, (2019) which is due to the same reason  
937 discussed for NPP comparison.



938  
939 Finally, our estimated total biomass enhancement ( $\Delta C_{veg}$ ) using JULES C/CN for the 1<sup>st</sup> and 15 years are in the  
940 middle range of C/CN models from Fleischer *et al.*, (2019) and in lower range of CNP models from Fleischer *et al.*  
941 *et al.*, (2019) using JULES CNP. Nevertheless, while JULES-CNP includes the trait-based parameters (Harper *et al.*  
942 *et al.*, 2016), other functions such as flexible C allocation and spatial variation of biomass turnover are still  
943 missing and future model improvement should be focused on their inclusion.

## 944 5. Conclusion

945  
946 Land ecosystems are a significant sink of atmospheric CO<sub>2</sub>, ergo buffering the anthropogenic increase of this  
947 flux. While tropical forests contribute substantially to the global land C sink, observational studies show that a  
948 stalled increase in carbon gains over the recent decade (Brienen *et al.*, 2015; Hubau *et al.*, 2020). However  
949 modelling studies that lack representation of P cycling processes predict an increasing sink (Fernández-Martínez  
950 *et al.*, 2019; Fleischer *et al.*, 2019). This is particularly relevant for efforts to mitigate dangerous climate change  
951 and assumptions on the future efficacy of the land C sink. Therefore, in this study, we presented the full  
952 terrestrial P cycling and its feedback on the C cycle within the JULES framework. Our results show that the  
953 model is capable of representing plant and soil P pools and fluxes at a site in Central Amazon. Moreover, the  
954 model estimated a significant NPP limitation under ambient CO<sub>2</sub>, due to the high P deficiency at this site which  
955 is representative of Central Amazon, and elevated CO<sub>2</sub> resulted in a further subsequent decrease in the land C  
956 sink capacity relative to the model without P limitation. While our study is a step toward the full nutrient cycling  
957 representation in ESMs, it can also help the empirical community to test different hypotheses (i.e., dynamic  
958 allocation and stoichiometry) and generate targeted experimental measurements (Medlyn *et al.*, 2015).

### 959 Code availability

960  
961 The modified version of JULES vn5\_5 and the P extension developed for this paper are freely available on Met  
962 Office Science Repository Service:  
963 [https://code.metoffice.gov.uk/svn/jules/main/branches/dev/mahdinakhavali/vn5.5\\_JULES\\_PM\\_NAKHAVALI/](https://code.metoffice.gov.uk/svn/jules/main/branches/dev/mahdinakhavali/vn5.5_JULES_PM_NAKHAVALI/)  
964 after registration ([http://jules-lsm.github.io/access\\_req/JULES\\_access.html](http://jules-lsm.github.io/access_req/JULES_access.html)) and completion of software license  
965 form. Codes for compiling model available at: (<https://doi.org/10.5281/zenodo.5711160>). Simulations were  
966 conducted using two sets of model configurations (namelists): ambient CO<sub>2</sub> condition  
967 (<https://doi.org/10.5281/zenodo.5711144>) and elevated CO<sub>2</sub> condition  
968 (<https://doi.org/10.5281/zenodo.5711150>).

### 969 Data availability

970  
971 The model outputs related to the results in this paper are provided on Zenodo repository  
972 (<https://doi.org/10.5281/zenodo.5710898>). All the R scripts used for processing the model outputs and  
973 producing results in form of table or figures are provided on Zenodo repository  
974 (<https://doi.org/10.5281/zenodo.5710896>).

975 *Author contributions.* MAN, LMM, SS, SEC, CAQ, AJW, IAP, KMA and DBC developed the model, per-  
976 formed simulations and analysis. CAQ, FVC, RP, LFL, KMA, GR, LS, ACMM, JSR, RA and JLC provided the  
977 measurements for the model parasitisation and evaluation. MAN, LMM, SS, IAP, SEC, FVC, RP, LFL, KMA  
978 and DBC contributed in writing the manuscript.

979 *Competing interests.* The authors declare no competing interests

980  
981 *Acknowledgments.* This work and its contributors (MAN, LMM, KMA and IPH) were supported by the UK  
982 Natural Environment Research Council (NERC) grant no NE/LE007223/1. MAN, LMM, SS, IPH were also  
983 supported by the Newton Fund through the Met Office Climate Science for Service Partnership Brazil (CSSP  
984 Brazil). LMM acknowledges support from the Natural Environment Research Council, grant NEC05816 LTS-  
985 M-UKESM. LFL was also supported by AmazonFACE programme (CAPES) and the National Institute of  
986 Amazonian Research, grant no: 88887.154643/2017-00. The authors acknowledge contributions from Celso  
987 Von Randow towards data curation of the meteorological forcing used in this study and Daniel Goll for  
988 modelling insight. We would like to thank Alessandro C. de Araújo and the Large-Scale Biosphere-Atmosphere  
989 Program (LBA), coordinated by the National Institute for Amazon Researches (INPA), for the use and  
990 availability of data.

992 **References:**

- 993
- 994 Aerts, R. and Chapin, F. S. (1999) 'The Mineral Nutrition of Wild Plants Revisited: A Re-evaluation of
- 995 Processes and Patterns', *Advances in Ecological Research*, 30(C), pp. 1–67. doi: 10.1016/S0065-
- 996 2504(08)60016-1.
- 997 Anav, A. *et al.* (2013) 'Evaluating the land and ocean components of the global carbon cycle in the CMIP5 earth
- 998 system models', *Journal of Climate*, 26(18), pp. 6801–6843. doi: 10.1175/JCLI-D-12-00417.1.
- 999 Aragão, L. E. O. C. *et al.* (2009) 'Above- and below-ground net primary productivity across ten Amazonian
- 1000 forests on contrasting soils', *Biogeosciences Discussions*, 6(1), pp. 2441–2488. doi: 10.5194/bgd-6-2441-2009.
- 1001 Araçõ, L. E. O. C. *et al.* (2009) 'Above- and below-ground net primary productivity across ten Amazonian
- 1002 forests on contrasting soils', *Biogeosciences*, 6(12), pp. 2759–2778. doi: 10.5194/bg-6-2759-2009.
- 1003 Araújo, A. C. *et al.* (2002) 'Comparative measurements of carbon dioxide fluxes from two nearby towers in a
- 1004 central Amazonian rainforest: The Manaus LBA site', *Journal of Geophysical Research*, 107(D20), p. 8090.
- 1005 doi: 10.1029/2001JD000676.
- 1006 Argles, A. P. K. *et al.* (2020) 'Robust Ecosystem Demography (RED version 1.0): A parsimonious approach to
- 1007 modelling vegetation dynamics in Earth system models', *Geoscientific Model Development*, 13(9), pp. 4067–
- 1008 4089. doi: 10.5194/gmd-13-4067-2020.
- 1009 Arora, V. K. *et al.* (2020) 'Carbon–concentration and carbon–climate feedbacks in CMIP6 models and their
- 1010 comparison to CMIP5 models', *Biogeosciences*, 17(16), pp. 4173–4222. doi: 10.5194/bg-17-4173-2020.
- 1011 Baig, S. *et al.* (2015) 'Does the growth response of woody plants to elevated CO<sub>2</sub> increase with temperature? A
- 1012 model-oriented meta-analysis', *Global Change Biology*, 21(12), pp. 4303–4319. doi: 10.1111/gcb.12962.
- 1013 Baker, T. R. *et al.* (2004) 'Variation in wood density determines spatial patterns in Amazonian forest biomass',
- 1014 *Global Change Biology*, 10(5), pp. 545–562. doi: 10.1111/j.1365-2486.2004.00751.x.
- 1015 Bentsen, M. *et al.* (2013) 'The Norwegian Earth System Model, NorESM1-M – Part 1: Description and basic
- 1016 evaluation of the physical climate', *Geoscientific Model Development*, 6(3), pp. 687–720. doi: 10.5194/gmd-6-
- 1017 687-2013.
- 1018 Best, M. J. *et al.* (2011) 'The Joint UK Land Environment Simulator (JULES), model description – Part 1:
- 1019 Carbon fluxes and vegetation dynamics', *Geoscientific Model Development*, 4(3), pp. 701–722. doi:
- 1020 10.5194/gmd-4-701-2011.
- 1021 Bradford, M. A. and Crowther, T. W. (2013) 'Carbon use efficiency and storage in terrestrial ecosystems', *New*
- 1022 *Phytologist*, 199(1), pp. 7–9. doi: 10.1111/nph.12334.
- 1023 Brienen, R. J. W. *et al.* (2015) 'Long-term decline of the Amazon carbon sink', *Nature*, 519(7543), pp. 344–
- 1024 348. doi: 10.1038/nature14283.
- 1025 Bruijnzeel, L. A. (1991) 'Nutrient input—output budgets of tropical forest ecosystems: A review', *Journal of*
- 1026 *Tropical Ecology*, 7(1), pp. 1–24. doi: 10.1017/S0266467400005010.
- 1027 Burke, E. J., Chadburn, S. E. and Ekici, A. (2017) 'A vertical representation of soil carbon in the JULES land
- 1028 surface scheme (vn4.3-permafrost) with a focus on permafrost regions', *Geoscientific Model Development*,
- 1029 10(2), pp. 959–975. doi: 10.5194/gmd-10-959-2017.
- 1030 Castanho, A. D. A. *et al.* (2013) 'Improving simulated Amazon forest biomass and productivity by including
- 1031 spatial variation in biophysical parameters', *Biogeosciences*, 10(4), pp. 2255–2272. doi: 10.5194/bg-10-2255-
- 1032 2013.
- 1033 Chapin, F. S. *et al.* (2011) *Principles of Terrestrial Ecosystem Ecology*. Springer New York (Biomedical and
- 1034 Life Sciences). Available at: <https://books.google.co.uk/books?id=68nFNpceRmIC>.
- 1035 Chave, J. *et al.* (2014) 'Improved allometric models to estimate the aboveground biomass of tropical trees',
- 1036 *Global Change Biology*, 20(10), pp. 3177–3190. doi: 10.1111/gcb.12629.
- 1037 Clark, D. B. *et al.* (2011) 'The Joint UK Land Environment Simulator (JULES), model description – Part 2:
- 1038 Carbon fluxes and vegetation dynamics', *Geoscientific Model Development*, 4(3), pp. 701–722. doi:
- 1039 10.5194/gmd-4-701-2011.
- 1040 Collatz, G. J. *et al.* (1991) 'Physiological and environmental regulation of stomatal conductance, photosynthesis
- 1041 and transpiration: a model that includes a laminar boundary layer', *Agricultural and Forest Meteorology*, 54(2–
- 1042 4), pp. 107–136. doi: 10.1016/0168-1923(91)90002-8.
- 1043 Collatz, G., Ribas-Carbo, M. and Berry, J. (1992) 'Coupled Photosynthesis-Stomatal Conductance Model for
- 1044 Leaves of C<sub>4</sub> Plants', *Functional Plant Biology*, 19(5), p. 519. doi: 10.1071/pp9920519.
- 1045 Comins, H. N. and McMurtrie, R. E. (1993) 'Long-Term Response of Nutrient-Limited Forests to CO<sub>2</sub>
- 1046 Enrichment; Equilibrium Behavior of Plant-Soil Models', *Ecological Applications*, 3(4), pp. 666–681. doi:
- 1047 10.2307/1942099.
- 1048 Costa, M. G. *et al.* (2016) 'Labile and Non-Labile Fractions of Phosphorus and Its Transformations in Soil
- 1049 under Eucalyptus', pp. 1–15. doi: 10.3390/f7010015.
- 1050 DeLuca, T. H., Keeney, D. R. and McCarty, G. W. (1992) 'Effect of freeze-thaw-events on mineralization of
- 1051 soil nitrogen', *Biol. Fertil. Soils*, 14, pp. 116–120. doi: 10.1007/BF00336260.

1052 Ellsworth, D. S. *et al.* (2017) ‘Elevated CO<sub>2</sub> does not increase eucalypt forest productivity on a low-phosphorus  
1053 soil’, *Nature Climate Change*, 7(4), pp. 279–282. doi: 10.1038/nclimate3235.

1054 Elser, J. J. *et al.* (2007) ‘Global analysis of nitrogen and phosphorus limitation of primary producers in  
1055 freshwater, marine and terrestrial ecosystems’, *Ecology Letters*, 10(12), pp. 1135–1142. doi: 10.1111/j.1461-  
1056 0248.2007.01113.x.

1057 Fernández-Martínez, M. *et al.* (2019) ‘Global trends in carbon sinks and their relationships with CO<sub>2</sub> and  
1058 temperature’, *Nature Climate Change*, 9(1), pp. 73–79. doi: 10.1038/s41558-018-0367-7.

1059 Fleischer, K. *et al.* (2019) ‘Amazon forest response to CO<sub>2</sub> fertilization dependent on plant phosphorus  
1060 acquisition’, *Nature Geoscience*. doi: 10.1038/s41561-019-0404-9.

1061 Friedlingstein, P. *et al.* (2006) ‘Climate-carbon cycle feedback analysis: Results from the C4MIP model  
1062 intercomparison’, *Journal of Climate*, 19(14), pp. 3337–3353. doi: 10.1175/JCLI3800.1.

1063 Friedlingstein, P. *et al.* (2019) ‘Comment on “The global tree restoration potential”’, *Science*. doi:  
1064 10.1126/science.aay8060.

1065 Fyllas, N. M. *et al.* (2009) ‘Basin-wide variations in foliar properties of Amazonian forest: phylogeny, soils and  
1066 climate’, *Biogeosciences*, 6(11), pp. 2677–2708. doi: 10.5194/bg-6-2677-2009.

1067 Gentile, R. *et al.* (2012) ‘Effects of long-term exposure to enriched CO<sub>2</sub> on the nutrient-supplying capacity of a  
1068 grassland soil’, *Biology and Fertility of Soils*, 48(3), pp. 357–362. doi: <http://dx.doi.org/10.1007/s00374-011-0616-7>.

1069 Goll, D. S. *et al.* (2017) ‘A representation of the phosphorus cycle for ORCHIDEE (revision 4520)’,  
1070 *Geoscientific Model Development*, 10(10), pp. 3745–3770. doi: 10.5194/gmd-10-3745-2017.

1071 Harper, A. B. *et al.* (2016) ‘Improved representation of plant functional types and physiology in the Joint UK  
1072 Land Environment Simulator (JULES v4.2) using plant trait information’, *Geoscientific Model Development*,  
1073 9(7), pp. 2415–2440. doi: 10.5194/gmd-9-2415-2016.

1074 Hatfield, J. L. and Dold, C. (2019) ‘Water-use efficiency: Advances and challenges in a changing climate’,  
1075 *Frontiers in Plant Science*, 10(February), pp. 1–14. doi: 10.3389/fpls.2019.00103.

1076 Haverd, V. *et al.* (2018) ‘A new version of the CABLE land surface model (Subversion revision r4601)  
1077 incorporating land use and land cover change, woody vegetation demography, and a novel optimisation-based  
1078 approach to plant coordination of photosynthesis’, *Geoscientific Model Development*, 11(7), pp. 2995–3026.  
1079 doi: 10.5194/gmd-11-2995-2018.

1080 He, M. and Dijkstra, F. A. (2014) ‘Drought effect on plant nitrogen and phosphorus: A meta-analysis’, *New  
1081 Phytologist*, 204(4), pp. 924–931. doi: 10.1111/nph.12952.

1082 Hedley, M. J., Stewart, J. W. B. and Chauhan, B. S. (1982) ‘Changes in Inorganic and Organic Soil Phosphorus  
1083 Fractions Induced by Cultivation Practices and by Laboratory Incubations’, *Soil Science Society of America  
1084 Journal*, 46(5), pp. 970–976. doi: <https://doi.org/10.2136/sssaj1982.03615995004600050017x>.

1085 Hou, E. *et al.* (2019) ‘Quantifying Soil Phosphorus Dynamics: A Data Assimilation Approach’, *Journal of  
1086 Geophysical Research: Biogeosciences*, 124(7), pp. 2159–2173. doi: 10.1029/2018JG004903.

1087 Hou, E. *et al.* (2020) ‘Global meta-analysis shows pervasive phosphorus limitation of aboveground plant  
1088 production in natural terrestrial ecosystems’, *Nature Communications*, 11(1), pp. 1–9. doi: 10.1038/s41467-020-  
1089 14492-w.

1090 Hubau, W. *et al.* (2020) ‘Asynchronous carbon sink saturation in African and Amazonian tropical forests’,  
1091 *Nature*, 579(7797), pp. 80–87. doi: 10.1038/s41586-020-2035-0.

1092 Hungate, B. a *et al.* (2003) ‘Nitrogen and Climate Change’, *Science*, 302(November), pp. 1512–1513.

1093 Jenkinson, D. S. *et al.* (1990) ‘The turnover of organic carbon and nitrogen in soil’, *The Royal Society*,  
1094 329(1255). doi: <https://doi.org/10.1098/rstb.1990.0177>.

1095 Jenkinson, D. S. and Coleman, K. (2008) ‘The turnover of organic carbon in subsoils. Part 2. Modelling carbon  
1096 turnover’, *European Journal of Soil Science*, 59(2), pp. 400–413. doi: 10.1111/j.1365-2389.2008.01026.x.

1097 Ji, D. *et al.* (2014) ‘Description and basic evaluation of Beijing Normal University Earth System Model (BNU-  
1098 ESM) version 1’, *Geoscientific Model Development*, 7(5), pp. 2039–2064. doi: 10.5194/gmd-7-2039-2014.

1099 Jiang, M. *et al.* (2019) ‘Towards a more physiological representation of vegetation phosphorus processes in land  
1100 surface models’, *New Phytologist*, 222(3), pp. 1223–1229. doi: 10.1111/nph.15688.

1101 Jiang, M. *et al.* (2020) ‘The fate of carbon in a mature forest under carbon dioxide enrichment’, *Nature*,  
1102 580(7802), pp. 227–231. doi: 10.1038/s41586-020-2128-9.

1103 Johnson, M. O. *et al.* (2016) ‘Variation in stem mortality rates determines patterns of above-ground biomass in  
1104 Amazonian forests: implications for dynamic global vegetation models’, *Global Change Biology*, 22(12), pp.  
1105 3996–4013. doi: 10.1111/gcb.13315.

1106 Jones, S. *et al.* (2020) ‘The impact of a simple representation of non-structural carbohydrates on the simulated  
1107 response of tropical forests to drought’, *Biogeosciences*, 17(13), pp. 3589–3612. doi: 10.5194/bg-17-3589-2020.

1108 Kattge, J. *et al.* (2009) ‘Quantifying photosynthetic capacity and its relationship to leaf nitrogen content for  
1109 global-scale terrestrial biosphere models’, *Global Change Biology*, 15(4), pp. 976–991. doi:  
1110 <https://doi.org/10.1111/j.1365-2486.2008.01744.x>.

1111

1112 Keller, M. *et al.* (2004) ‘Ecological research in the Large-scale Biosphere-Atmosphere Experiment in  
1113 Amazonia: Early results’, *Ecological Applications*, 14(4 SUPPL.), pp. 3–16. doi: 10.1890/03-6003.

1114 Klein, T. *et al.* (2016) ‘Growth and carbon relations of mature *Picea abies* trees under 5 years of free-air CO<sub>2</sub>  
1115 enrichment’, *Journal of Ecology*, 104(6), pp. 1720–1733. doi: 10.1111/1365-2745.12621.

1116 Koch, A., Hubau, W. and Lewis, S. L. (2021) ‘Earth System Models Are Not Capturing Present-Day Tropical  
1117 Forest Carbon Dynamics’, *Earth’s Future*, 9(5), pp. 1–19. doi: 10.1029/2020EF001874.

1118 Körner, C. *et al.* (2005) ‘Ecology: Carbon flux and growth in mature deciduous forest trees exposed to elevated  
1119 CO<sub>2</sub>’, *Science*, 309(5739), pp. 1360–1362. doi: 10.1126/science.1113977.

1120 Van Langenhove, L. *et al.* (2020) ‘Atmospheric deposition of elements and its relevance for nutrient budgets of  
1121 tropical forests’, *Biogeochemistry*, 149(2), pp. 175–193. doi: 10.1007/s10533-020-00673-8.

1122 Lapola, D. M. and Norby, R. (2014) ‘Assessing the effects of increased atmospheric CO<sub>2</sub> on the ecology and  
1123 resilience of the Amazon forest’, *Science plan et implementation strategy*, AMAZON FAC.

1124 LeBauer, D. and Treseder, K. (2008) ‘Nitrogen Limitation of Net Primary Productivity’, *Ecology*, 89(2), pp.  
1125 371–379.

1126 Lloyd, J. *et al.* (2001) ‘Should Phosphorus Availability Be Constraining Moist Tropical Forest Responses to  
1127 Increasing CO<sub>2</sub> Concentrations?’, in *Global Biogeochemical Cycles in the Climate System*. Elsevier, pp. 95–  
1128 114. doi: 10.1016/B978-012631260-7/50010-8.

1129 Long, M. C. *et al.* (2013) ‘Twentieth-century oceanic carbon uptake and storage in CESM1(BGC)’, *Journal of*  
1130 *Climate*, 26(18), pp. 6775–6800. doi: 10.1175/JCLI-D-12-00184.1.

1131 De Lucia, E. H. *et al.* (2007) ‘Forest carbon use efficiency: Is respiration a constant fraction of gross primary  
1132 production?’, *Global Change Biology*, 13(6), pp. 1157–1167. doi: 10.1111/j.1365-2486.2007.01365.x.

1133 Lugli, L. F. (2013) *Estoque de nutrientes na serrapilheira fina e grossa em função de fatores edáficos em*  
1134 *florestas do Amazonas, Brasil*. Instituto Nacional de Pesquisas da Amazônia - INPA. Available at:  
1135 <https://repositorio.inpa.gov.br/handle/1/5028>.

1136 Lugli, L. F. *et al.* (2020) ‘Multiple phosphorus acquisition strategies adopted by fine roots in low-fertility soils  
1137 in Central Amazonia’, *Plant and Soil*, 450(1–2), pp. 49–63. doi: 10.1007/s11104-019-03963-9.

1138 Lugli, L. F. *et al.* (2021) ‘Rapid responses of root traits and productivity to phosphorus and cation additions in a  
1139 tropical lowland forest in Amazonia’, *New Phytologist*, 230(1), pp. 116–128. doi: 10.1111/nph.17154.

1140 Luo, Y. *et al.* (2004) ‘Progressive nitrogen limitation of ecosystem responses to rising atmospheric carbon  
1141 dioxide’, *BioScience*, 54(8), pp. 731–739. doi: 10.1641/0006-3568(2004)054[0731:PNLOER]2.0.CO;2.

1142 Malhi, Y. *et al.* (2004) ‘The above-ground coarse wood productivity of 104 Neotropical forest plots’, *Global*  
1143 *Change Biology*, 10(5), pp. 563–591. doi: 10.1111/j.1529-8817.2003.00778.x.

1144 Malhi, Y. *et al.* (2006) ‘The regional variation of aboveground live biomass in old-growth Amazonian forests’,  
1145 *Global Change Biology*, 12(7), pp. 1107–1138. doi: 10.1111/j.1365-2486.2006.01120.x.

1146 Malhi, Y. *et al.* (2009) ‘Comprehensive assessment of carbon productivity, allocation and storage in three  
1147 Amazonian forests’, *Global Change Biology*, 15(5), pp. 1255–1274. doi: 10.1111/j.1365-2486.2008.01780.x.

1148 Malhi, Y. (2012) ‘The productivity, metabolism and carbon cycle of tropical forest vegetation’, *Journal of*  
1149 *Ecology*, 100(1), pp. 65–75. doi: 10.1111/j.1365-2745.2011.01916.x.

1150 Malhi, Y., Doughty, C. and Galbraith, D. (2011) ‘The allocation of ecosystem net primary productivity in  
1151 tropical forests’, *Philosophical Transactions of the Royal Society B: Biological Sciences*, 366(1582), pp. 3225–  
1152 3245. doi: 10.1098/rstb.2011.0062.

1153 Martins, N. P. *et al.* (2021) ‘Fine roots stimulate nutrient release during early stages of leaf litter decomposition  
1154 in a Central Amazon rainforest’, *Plant and Soil*, 469(1–2), pp. 287–303. doi: 10.1007/s11104-021-05148-9.

1155 Medlyn, B. E. *et al.* (2015) ‘Using ecosystem experiments to improve vegetation models’, *Nature Climate*  
1156 *Change*, 5(6), pp. 528–534. doi: 10.1038/nclimate2621.

1157 Medlyn, B. E. *et al.* (2016) ‘Using models to guide field experiments: a priori predictions for the CO<sub>2</sub> response  
1158 of a nutrient- and water-limited native Eucalypt woodland’, *Global Change Biology*, 22(8), pp. 2834–2851. doi:  
1159 10.1111/gcb.13268.

1160 Mercado, L. M. *et al.* (2011) ‘Variations in Amazon forest productivity correlated with foliar nutrients and  
1161 modelled rates of photosynthetic carbon supply’, *Philosophical Transactions of the Royal Society B: Biological*  
1162 *Sciences*, 366(1582), pp. 3316–3329. doi: 10.1098/rstb.2011.0045.

1163 Mitchard, E. T. A. (2018) ‘The tropical forest carbon cycle and climate change’, *Nature*, 559(7715), pp. 527–  
1164 534. doi: 10.1038/s41586-018-0300-2.

1165 Neff, J. C., Hobbie, S. E. and Vitousek, P. M. (2000) ‘Nutrient and mineralogical control on dissolved organic  
1166 C, N and P fluxes and stoichiometry in Hawaiian soils’, *Biogeochemistry*, 51(3), pp. 283–302. doi:  
1167 10.1023/A:1006414517212.

1168 Norby, R. J. *et al.* (2016) ‘Model–data synthesis for the next generation of forest free-air <sc>CO</sc><sub>2</sub>  
1169 enrichment ( <sc>FACE</sc> ) experiments’, *New Phytologist*, 209(1), pp. 17–28. doi: 10.1111/nph.13593.

1170 Nordin, A., Högberg, P. and Näsholm, T. (2001) ‘Soil nitrogen form and plant nitrogen uptake along a boreal  
1171 forest productivity gradient’, *Oecologia*, 129(1), pp. 125–132. doi: 10.1007/s004420100698.

1172 Pan, Y. *et al.* (2011) ‘A Large and Persistent Carbon Sink in the World’s Forests’, *Science*, 333(6045), pp. 988–  
1173 993. doi: 10.1126/science.1201609.

1174 Perakis, S. S. and Hedin, L. O. (2002) ‘Nitrogen loss from unpolluted South American forests mainly via  
1175 dissolved organic compounds’, *Nature*, 415(6870), pp. 416–419. doi: 10.1038/415416a.

1176 Phillips, O. L. *et al.* (2004) ‘Pattern and process in Amazon tree turnover, 1976–2001’, *Philosophical  
1177 Transactions of the Royal Society B: Biological Sciences*, 359(1443), pp. 381–407. doi: 10.1098/rstb.2003.1438.

1178 Phillips, O. L. *et al.* (2017) ‘Carbon uptake by mature Amazon forests has mitigated Amazon nations’ carbon  
1179 emissions’, *Carbon Balance and Management*, 12(1), pp. 1–9. doi: 10.1186/s13021-016-0069-2.

1180 Quesada, C. A. *et al.* (2010) ‘Variations in chemical and physical properties of Amazon forest soils in relation to  
1181 their genesis’, *Biogeosciences*, 7(5), pp. 1515–1541. doi: 10.5194/bg-7-1515-2010.

1182 Quesada, C. A. *et al.* (2011) ‘Soils of Amazonia with particular reference to the RAINFOR sites’,  
1183 *Biogeosciences*, 8(6), pp. 1415–1440. doi: 10.5194/bg-8-1415-2011.

1184 Quesada, C. A. *et al.* (2012) ‘Basin-wide variations in Amazon forest structure and function are mediated by  
1185 both soils and climate’, *Biogeosciences*, 9(6), pp. 2203–2246. doi: 10.5194/bg-9-2203-2012.

1186 Reed, S. C., Yang, X. and Thornton, P. E. (2015) ‘Incorporating phosphorus cycling into global modeling  
1187 efforts: A worthwhile, tractable endeavor’, *New Phytologist*, 208(2), pp. 324–329. doi: 10.1111/nph.13521.

1188 Ryan, M. G. (2013) ‘Three decades of research at Flakaliden advancing whole-tree physiology, forest ecosystem  
1189 and global change research’, *Tree Physiology*, 33(11), pp. 1123–1131. doi: 10.1093/treephys/tpt100.

1190 Sampaio, G. *et al.* (2021) ‘CO<sub>2</sub> physiological effect can cause rainfall decrease as strong as large-scale  
1191 deforestation in the Amazon’, *Biogeosciences*, 18(8), pp. 2511–2525. doi: 10.5194/bg-18-2511-2021.

1192 Sanchez, P. A. (1977) ‘Properties and Management of Soils in the Tropics’, *Soil Science*, 124(3). Available at:  
1193 [https://journals.lww.com/soilsci/Fulltext/1977/09000/Properties\\_and\\_Management\\_of\\_Soils\\_in\\_the\\_Tropics.12.aspx](https://journals.lww.com/soilsci/Fulltext/1977/09000/Properties_and_Management_of_Soils_in_the_Tropics.12.aspx).  
1194

1195 Sardans, J., Rivas-Ubach, A. and Peñuelas, J. (2012) ‘The C:N:P stoichiometry of organisms and ecosystems in  
1196 a changing world: A review and perspectives’, *Perspectives in Plant Ecology, Evolution and Systematics*, 14(1),  
1197 pp. 33–47. doi: 10.1016/j.ppees.2011.08.002.

1198 Schimel, D., Stephens, B. B. and Fisher, J. B. (2015) ‘Effect of increasing CO<sub>2</sub> on the terrestrial carbon cycle’,  
1199 *Proceedings of the National Academy of Sciences of the United States of America*, 112(2), pp. 436–441. doi:  
1200 10.1073/pnas.1407302112.

1201 Shen, J. *et al.* (2011) ‘Phosphorus dynamics: From soil to plant’, *Plant Physiology*, 156(3), pp. 997–1005. doi:  
1202 10.1104/pp.111.175232.

1203 Sitch, S. *et al.* (2008) ‘Evaluation of the terrestrial carbon cycle, future plant geography and climate-carbon  
1204 cycle feedbacks using five Dynamic Global Vegetation Models (DGVMs)’, *Global Change Biology*, 14(9), pp.  
1205 2015–2039. doi: 10.1111/j.1365-2486.2008.01626.x.

1206 Stephenson, N. L. and Van Mantgem, P. J. (2005) ‘Forest turnover rates follow global and regional patterns of  
1207 productivity’, *Ecology Letters*, 8(5), pp. 524–531. doi: 10.1111/j.1461-0248.2005.00746.x.

1208 Sun, Y. *et al.* (2021) ‘Global evaluation of the nutrient-enabled version of the land surface model ORCHIDEE-  
1209 CNP v1.2 (r5986)’, *Geoscientific Model Development*, 14(4), pp. 1987–2010. doi: 10.5194/gmd-14-1987-2021.

1210 Vicca, S. *et al.* (2012) ‘Fertile forests produce biomass more efficiently’, *Ecology Letters*, 15(6), pp. 520–526.  
1211 doi: 10.1111/j.1461-0248.2012.01775.x.

1212 Vitousek, P. M. *et al.* (1997) ‘Human Domination of Earth Ecosystems’, *Science*, 278(5335), p. 21. Available  
1213 at: <http://www.cheric.org/research/tech/periodicals/view.php?seq=257860>.

1214 Vitousek, P. M. *et al.* (2010) ‘Terrestrial phosphorus limitation: Mechanisms, implications, and nitrogen-  
1215 phosphorus interactions’, *Ecological Applications*, 20(1), pp. 5–15. doi: 10.1890/08-0127.1.

1216 Vitousek, P. M. and Howarth, R. W. (1991) ‘Nitrogen limitation on land and in the sea: How can it occur?’,  
1217 *Biogeochemistry*, 13(2), pp. 87–115. doi: 10.1007/BF00002772.

1218 Walker, A. P. *et al.* (2021) ‘Integrating the evidence for a terrestrial carbon sink caused by increasing  
1219 atmospheric CO<sub>2</sub>’, *New Phytologist*, 229(5), pp. 2413–2445. doi: 10.1111/nph.16866.

1220 Walker, T. W. and Syers, J. K. (1976) ‘The fate of phosphorus during pedogenesis’, *Geoderma*, 15(1), pp. 1–19.  
1221 doi: 10.1016/0016-7061(76)90066-5.

1222 Wang, Y. P., Houlton, B. Z. and Field, C. B. (2007) ‘A model of biogeochemical cycles of carbon, nitrogen, and  
1223 phosphorus including symbiotic nitrogen fixation and phosphatase production’, *Global Biogeochemical Cycles*,  
1224 21(1), pp. 1–15. doi: 10.1029/2006GB002797.

1225 Wang, Y. P., Law, R. M. and Pak, B. (2010) ‘A global model of carbon, nitrogen and phosphorus cycles for the  
1226 terrestrial biosphere’, *Biogeosciences*, 7(7), pp. 2261–2282. doi: 10.5194/bg-7-2261-2010.

1227 Went, F. W. and Stark, N. (1968) ‘Mycorrhiza’, *BioScience*, 18(11), pp. 1035–1039. doi: 10.2307/1294552.

1228 Wiltshire, A. J. *et al.* (2021) ‘Jules-cn: A coupled terrestrial carbon-nitrogen scheme (jules vn5.1)’,  
1229 *Geoscientific Model Development*, 14(4), pp. 2161–2186. doi: 10.5194/gmd-14-2161-2021.

1230 Xiao, J. *et al.* (2013) ‘Carbon fluxes, evapotranspiration, and water use efficiency of terrestrial ecosystems in  
1231 China’, *Agricultural and Forest Meteorology*, 182–183, pp. 76–90. doi: 10.1016/j.agrformet.2013.08.007.

1232 Xu, Z. *et al.* (2016) 'Elevated-CO<sub>2</sub> response of stomata and its dependence on environmental factors', *Frontiers*  
1233 *in Plant Science*, 7(MAY2016), pp. 1–15. doi: 10.3389/fpls.2016.00657.  
1234 Yang, X. *et al.* (2013) 'The distribution of soil phosphorus for global biogeochemical modeling',  
1235 *Biogeosciences*, 10(4), pp. 2525–2537. doi: 10.5194/bg-10-2525-2013.  
1236 Yang, X. *et al.* (2014) 'The role of phosphorus dynamics in tropical forests – a modeling study using CLM-  
1237 CNP', *Biogeosciences*, 11(6), pp. 1667–1681. doi: 10.5194/bg-11-1667-2014.  
1238 Yang, X. and Post, W. M. (2011) 'Phosphorus transformations as a function of pedogenesis: A synthesis of soil  
1239 phosphorus data using Hedley fractionation method', *Biogeosciences*, 8(10), pp. 2907–2916. doi: 10.5194/bg-8-  
1240 2907-2011.  
1241 Zaehle, S. and Dalmonech, D. (2011) 'Carbon-nitrogen interactions on land at global scales: Current  
1242 understanding in modelling climate biosphere feedbacks', *Current Opinion in Environmental Sustainability*,  
1243 3(5), pp. 311–320. doi: 10.1016/j.cosust.2011.08.008.  
1244 Zaehle, S. and Friend, A. D. (2010) 'Carbon and nitrogen cycle dynamics in the O-CN land surface model: 1.  
1245 Model description, site-scale evaluation, and sensitivity to parameter estimates', *Global Biogeochemical Cycles*,  
1246 24(1), pp. 1–13. doi: 10.1029/2009GB003521.  
1247 Zhu, Q. *et al.* (2016) 'Multiple soil nutrient competition between plants, microbes, and mineral surfaces: model  
1248 development, parameterization, and example applications in several tropical forests', *Biogeosciences*, 13(1), pp.  
1249 341–363. doi: 10.5194/bg-13-341-2016.  
1250